R. & M. No. 3577

R. & M. No. 3577

MINISTRY OF TECHNOLOGY

AERONAUTICAL RESEARCH COUNCIL
REPORTS AND MEMORANDA

Flight Measurements of the Lift, Longitudinal Trim and Drag of the Fairey Delta 2 at Mach Numbers up to 1·65 and Comparisons with Wind-Tunnel Results

By R. Rose, C. S. Barnes
and
A. A. Woodfield

Aerodynamics Dept., R.A.E., Bedford

Flight Measurements of the Lift, Longitudinal Trim and Drag of the Fairey Delta 2 at Mach Numbers up to 1·65 and Comparisons with Wind-Tunnel Results

By R. Rose, C. S. Barnes
and
A. A. Woodfield
Aerodynamics Dept., R.A.E., Bedford

Reports and Memoranda No. 3577*
June, 1967

Summary.

Measurements have been made on the Fairey Delta 2,60° delta research aircraft, mainly at 40 000 ft; some tests were made at lower altitudes to study aeroelastic effects. The main points from the results are as follows.

The trimmed lift-curve slope is independent of incidence, but the trim curves are non-linear for large elevator deflections. The relationship between the drag coefficient and the square of the lift coefficient is non-linear at subsonic speeds but linear at supersonic speeds. The effect of altitude on the trim and drag results is significant, apparently because of aileron rigged-up angle differences, and Reynolds number effects.

Comparison of flight and tunnel results shows good agreement for the slope of the trim curve, but there are significant differences in elevator angle. These differences are consistant with those found in the trimmed lift data and can not be completely explained in terms of the different aileron riggid-up angles in flight and tunnel. The lift and pitching moment are probably affected by the known difference between the development of the wing vortex in flight and tunnel.

Agreement between flight and tunnel values of the elevator pitching power, and trimmed and untrimmed lift-curve slopes is good although that for the pitching power may be fortuitous; that for elevator lifting power is fair. The increase in manoeuvre margin from subsonic to supersonic speed is smaller in flight.

*Replaces R.A.E. Tech. Report 67036—A.R.C. 29 542.

LIST OF CONTENTS

1. *Introduction.*

The Fairey Delta 2 is a 60° delta wing tailless research aircraft intended for investigation of the properties of this type of planform over a wide range of Mach number and lift coefficient.

This Report presents some flight measurements of lift, trim and drag made on the aircraft at R.A.E. Bedford. Comparisons are made with lift and trim measurements on 1/9[1,2] and 1/24[3,4] scale wind-tunnel models.

Drag measurements have been made on the 1/9 scale model, but in this Report flight/tunnel comparisons are only made of the induced-drag factor. The minimum drag coefficient has not been compared because it is necessary to allow for significant differences between the aircraft and the wind-tunnel model. Besides the obvious effects of Reynolds number on skin friction, the different values, between model and full-scale, of roughness drag, spillage drag, jet-efflux effects and non-representation of the intake boundary-layer bleeds have to be considered. A measure of the jet-efflux effect in flight on the rear fuselage pressures has been made and similar measurements have been made on the model.

2. *Description of Aircraft and Instrumentation.*

2.1. *Aircraft.*

The aircraft has a delta wing of aspect ratio 2, the wing leading edge is swept at 60° and the thickness-chord ratio 0·04. Table 1 gives the principal dimensions and leading details of the aircraft. Figs. 1 and 2 show a general arrangement and photograph of the aircraft. Primary control is by conventional elevators, ailerons and rudder; the ailerons are rigged up 3·2° relative to the wing chord; the aircraft has no flaps and has four petal airbrakes mounted on the rear fuselage. Propulsion is provided by a Rolls Royce Avon R.A. 28R turbojet engine; the jet-pipe nozzle has moveable eyelids which are fully open for reheat operation and which are moved to a closed position to reduce the nozzle area for non-reheat running. The only control over engine thrust, with reheat on, is by a limited throttling of the engine. The test-bed ratings of the engine and jet pipe are 9530 lb and 11 820 lb for non-reheat and reheat operation respectively. The thrust axis is inclined at 1° nose up relative to the fuselage datum.

2.2. *Instrumentation.*

The parameters measured relevant to the present tests were as follows:

Indicated airspeed
Altitude
Normal acceleration
Longitudinal acceleration
Incidence
Total temperature
Elevator angle
Engine rpm
Total fuel consumed
Fuel-flow rates (engine and reheat)
Transition pipe total temperature
Transition pipe total pressure
Transition pipe static pressure
Propelling nozzle static pressure.

A few measurements were made of the static pressure on the port side of the rear fuselage using surface pressure tape, along generators at $\pm 37°$ to the fuselage centreline plane, Fig. 21. Most of the pressure holes were on the airbrakes.

The tests were made in essentially non-stabilised conditions and any parameters which varied rapidly were recorded on Hussenot A.22 continuous-trace recorders. Parameters which only varied slowly were measured by standard instruments in an automatic observer. The accelerometers were carefully aligned along and perpendicular to the fuselage datum respectively.

2.3. *Measured Surface Defects.*

Because the state of the aircraft surface significantly affects the drag, a fairly detailed survey has been made of surface defects. These defects consist of small-scale surface irregularities, nominally flush rivet heads, detachable panels and control surface gaps. To obtain details of the number and size of the surface irregularities a number of casts were made of the aircraft surface for the positions shown in Fig. 3. More casts were taken of the upper wing surface than the lower as this surface appeared to be rougher. Table 2 summarises the height or depth and number of irregularities for the various wetted areas of the aircraft. The large number of irregularities per square foot on the fin and rudder are due to a poor local paint surface. The diameter and height of projection of the rivet heads has also been determined from the casts, although in this case the number of rivet heads per sample was small and consequently the number of rivets for each surface was obtained from a sample count over large areas. Table 3 summarises the rivet head data.

The aircraft has about 160 detachable panels and doors that are frequently removed for servicing and instrumentation requirements, the number and location of these panels and doors are summarised in Table 4 and Fig. 4. The projection of each panel above the local surface and its forward facing frontal area were measured. The total frontal area of the panel projections is 14·3 sq inches, the height of the projections varying between 0·005 inch and 0·025 inch.

Control surface gaps on the aircraft were sealed with felt strips. These strips did not seal the complete length of the controls; Table 5 gives data on the unsealed gaps.

3. *Flight Tests.*

Most of the flights were made at a nominal altitude of 40 000 ft within a variation of height of ± 2000 ft. However, for some of the flights the variation of height was much greater. Some tests were made at lower altitudes to investigate the effects of aeroelasticity. The range of Mach number covered was 0·7 to 1·65 at 40 000 ft and 0·55 to 1·2 at 10 000 ft. The Reynolds number at a Mach number of 1·0 was 32×10^6 at 40 000 ft and $89{\cdot}5 \times 10^6$ at 10 000 ft, based on the aerodynamic mean chord.

At subsonic speeds, tests were made with speed both stabilised and non-stabilised. Most of the non-stabilised tests were made in turns, but a few were made in 'push-over' manoeuvres to reduce the lift. The latter type of test was made as the results showed that at subsonic speeds the drag was not a linear function of the square of the lift coefficient. Without the 'push-over' results a large extrapolation of the data would have been required to evaluate the minimum drag coefficient. In supersonic flight the speed was varying continuously; this was caused by either an excess of thrust in level flight giving a longitudinal acceleration, or the increase of drag with normal acceleration giving a longitudinal deceleration. Although it would have been possible to stabilise some conditions at supersonic speeds by limited throttling of the engine with reheat on, the endurance of the aircraft is limited, and it is more economical in flight test time to accept varying speed rather than to stabilise by throttling. In a typical flight at 40 000 ft, reheat was selected on at $M = 0{\cdot}95$ and the aircraft was allowed to accelerate, in essentially level flight, up to about $M = 1{\cdot}65$. It was then pulled into a turn with the speed falling off due to the rapid increase of drag. In these supersonic decelerating turns reheat was left on to prevent too rapid a deceleration; thus only conditions with reheat on were recorded at supersonic speeds. At supersonic speeds the normal acceleration in turns was limited by the maximum available elevator angle to trim. With the limited amount of fuel available, a considerable number of flights were required to obtain results at supersonic speeds.

The tests were made over a fairly long period during which it might have been expected that structurally the aircraft could have suffered minor distortions. This is particularly relevant to the surface finish of the aircraft.

4. *Method of Analysis.*

4.1. *Determination of Engine Gross Thrust and Intake Momentum Drag.*

The gross thrust is the sum of the momentum and pressure forces at the final nozzle, and the intake momentum drag is the product of the air mass flow entering the engine and the aircraft true speed. The gross thrust and air mass flow were determined, following the methods of Ref. 5, from measurements of static pressure in the propelling nozzle, and total pressure, static pressure and total temperature in the

transition section between the turbine exit and reheat section. Application of this method requires knowledge of the effective areas of the transition pipe, A_4, and the propelling nozzle, A_5. These were determined from calibrations in sea level[5] and altitude[6] test beds at the N.G.T.E. at final nozzle pressure ratios representative of flight conditions and are shown in Figs. 5 and 6. The relatively small scatter of these calibrations should be noted.

4.2. *Determination of Lift and Drag.*

The lift and drag of the aircraft are calculated from the gross thrust, intake momentum drag, and the accelerations along and normal to the flight path. These accelerations are obtained by suitable vector addition of the readings of accelerometers aligned along and normal to the fuselage datum. The longitudinal accelerometer reading is corrected for the effects of cross acceleration using the calibration of Ref. 7.

The incidences corresponding to the values of lift and drag, are obtained from the incidence vane readings, corrected for the effects of boom distortion, boom upwash using the calibration of Ref. 8, and the theoretically estimated wing and fuselage upwash at subsonic speeds. The effect of pitching velocity on incidence was negligible.

The lift and drag forces follow from the equations

$$L = n\,W - F_G \sin(\alpha + 1), \tag{1}$$

$$D = F_G \cos(\alpha + 1) - \frac{Q_0\,V}{g} - W a_x \tag{2}$$

where the notation is explained in the list of symbols. Where necessary a constant increment of drag coefficient, $\Delta C_{D_p} = 0{\cdot}0008$, was subtracted from the measured drag to allow for the estimated drag of a swinging probe[5] at the rear of the aircraft on some flights.

4.3. *Control Surface Distortions.*

Both the elevator and aileron control surfaces are flexible, and as the control-surface transmitters are attached to the jack output, corrections must be made for this flexibility. The elevator jacks are in the fuselage, and operate the elevators *via* somewhat flexible links which are attached to torque tubes at the inboard ends of the elevators. In the case of the ailerons, the jack load is applied near the mid-span of the control *via* a short and very stiff linkage.

To assess the effective stiffness of the control surfaces, including the linkage, ground tests were made. In these tests uniform loading was applied to the control surfaces by lead-shot bags. Flight pressure-plotting tests[9] have shown that the loading is reasonably uniform for the elevators, but that this condition is not so representative for the ailerons. However, the error involved is not significant, since the effective stiffness of the ailerons is much larger than for the elevators.

Because of the difficulty of supporting and loading the complete aircraft in a representative fashion, the distortion of the controls and linkages was measured in ground rigs which utilised the control-surface hinges. In these rigs it was only possible to load the elevator and aileron to 300 lb ft and 1200 lb ft respectively which is only about 25 per cent of the maximum flight values. The local angular distortion, relative to the transducer position, was measured at the leading and trailing edges of the controls at several spanwise stations.

For the elevator, at a given spanwise station, the mean angular deflection of the section has been defined as the mean of the deflections at the leading and trailing edge. The mean angular deflection of the sections has been integrated, using a weighting function proportional to the chord, to give an overall mean control deflection angle. The effective stiffness of the elevator, including the jack linkage, obtained by dividing the applied moment by the mean deflection angle, is 2000 lb ft/degree. This stiffness is quite small, but flexibility of the linkage accounts for about two-thirds of the measured distortion, and the jack load is applied to one end of the elevator.

For the ailerons, the distortions were very small and the effective stiffness was about 40 000 lb ft/degree.

In this case, flexibility of the linkage was negligible, and the jack load was applied near the mid-span of the control.

5. *Results and Discussion of Flight Tests.*

The results of the flight tests are discussed in this section, and comparison with wind-tunnel results is made in Section 6.

Fig. 7 shows a time history of Mach number, C_D, C_{L_t}, incidence and elevator angle obtained from a typical record. Most records were sampled at approximately every 20 seconds corresponding to an instrumentation switching cycle required for a concurrent experiment. Similar records were obtained from the flight tests over a wide range of C_{L_t} and Mach number. To allow a detailed analysis of the results in the following sub-sections, data have been selected at various Mach numbers up to 1·65, a variation in Mach number of $\pm 0{\cdot}025$ being accepted at most speeds, except at $M = 0{\cdot}94$ and 0·97 where variations larger than $\pm 0{\cdot}015$ were discarded as the parameters were varying rapidly with Mach number.

Most of the tests were made with speed non-stabilised. However, at subsonic speeds, tests were made with speed both stabilised and non-stabilised, and comparison of results showed no apparent effect of longitudinal acceleration. At supersonic speeds it has not been possible to detect differences between results from accelerating and decelerating flight.

The airflow through the engine influences the lift, drag and trim of the aircraft. Fig. 8 shows that the non-dimensional air mass-flow parameter at maximum engine rpm, the condition for most of the flight tests, is almost constant.

The mean centre of gravity position for the tests was $0{\cdot}319\,\bar{c}$; the variation due to different fuel states was $\pm 0{\cdot}0025\,\bar{c}$.

5.1. *Lift.*

Fig. 9 shows the variation of the trimmed lift coefficient with incidence for various Mach numbers. Data points are shown for the three test heights, 10 000 ft, 20 000 ft and 40 000 ft. Straight lines have been drawn using the least-squares method through the results at 40 000 ft; as there is only a limited amount of data at the lower altitudes no lines have been drawn through these results. There may be an effect of altitude on the results, but because of the scatter it is not possible to distinguish any significant effect except possibly at Mach numbers of 1·10 and 1·15. Even at these speeds there is no systematic trend with altitude, as the 10 000 ft and 20 000 ft results agree well amongst themselves but fall to the left of the 40 000 ft line. Effects of altitude could be due to either aeroelasticity or Reynolds number affecting the flow, or possibly both effects cancelling at 20 000 ft. Estimates by the aircraft manufacturer show that the effects of aeroelasticity should make the lift-curve slope at 10 000 ft about 4 per cent less than at 40 000 ft at $M = 1{\cdot}1$. Within the scatter of the results, it is not possible to see such a reduction in the lift-curve slope.

Andrews[10] shows differences between the untrimmed lift-curve slopes of the Fairey Delta 2 obtained at altitudes of 10 000 ft and 38 000 ft by analysis of longitudinal short-period oscillations of the aircraft. However, he considered that the 10 000 ft results were unreliable and that the measured differences were probably not genuine.

It is concluded that there is probably no significant effect of aeroelasticity on the trimmed lift, although there may be Reynolds number effects.

The trimmed lift-curve slope, $\frac{dC_{L_t}}{d\alpha}$, is shown in Fig. 10. The small variations between $M = 0{\cdot}9$ and 1·05 are probably not significant, but the peak at $M = 1{\cdot}1$ is thought to be genuine.

5.2. *Trim.*

Fig. 11 shows the variation of the elevator angle to trim, corrected for the effects of elevator flexibility, with lift coefficient for various Mach numbers. As in the case of the lift results (Fig. 9) lines have only been drawn through the 40 000 ft points. At subsonic speeds the elevator angle to trim is a linear function of C_{L_t} and straight lines have been drawn through the results by the least-squares method. At supersonic

speeds the trim curves become non-linear as lift increases. This is possibly due to a loss of elevator effectiveness at the larger elevator deflections as tunnel tests[1,2,3,4] show that the C_M versus C_L relationship is linear. There is an unmistakable effect of altitude on the results, the lower altitude results being offset by about one degree throughout the speed range. It is not believed that this effect is due to that usually associated with aeroelasticity, since this normally affects the aerodynamic-centre position, which would show as a change in slope of the trim curves. Estimates by the aircraft manufacturer gives a change in aerodynamic centre, from the high to low altitude conditions, of about $\frac{1}{2}$ per cent to 1 per cent $\bar{c}$. This would only change the slope of the trim curves by about 5 per cent which is within the scatter of the results. Estimates have shown that the effect of the thrust moment is not sufficient to explain the measured effect. The offset in the lower altitude trim curves must be caused by a change in C_{m_0}, the pitching-moment coefficient at zero lift. The primary cause of a C_{m_0} change must be a change in rigged-up angle of the ailerons. Fig. 12 shows that the rigged-up angle in flight changes from the ground setting and varies with flight conditions. This change is not thought to be due to aeroelastic distortion of the control surface as it is very stiff, but could be due to differential temperature effects in the control circuit or to distortion of the wing structure porting the hydraulic jack valves and thus moving the ailerons. Such a change would affect C_{m_0}, and thus may account for some of the change observed in elevator angle to trim at the different heights. Another possible reason for the change in C_{m_0} could be variation of the wing pressure distribution with altitude, at a given lift coefficient, affecting the trim of the aircraft. This effect has in fact been observed on part of the wing from steady pressure measurements in flight on the Fairey Delta 2 at subsonic speeds[9]; no comparable results are available at transonic or supersonic speeds.

5.3. *Elevator Effectiveness.*

Fig. 13 shows the variation of $-\left(\frac{d\eta}{dC_{L_t}}\right)$ with Mach number; this parameter has been deduced from the slope of the linear portion of the curves of Fig. 11 and increases from about 0·25 at subsonic speeds to 1·15 at $M = 1{\cdot}6$.

The elevator pitching power, $\left(\frac{\partial C_m}{\partial \eta}\right)_{C_L}$, at a fixed Mach number, is given by

$$\left(\frac{\partial C_m}{\partial \eta}\right)_{C_L} = \left(\frac{\partial C_M}{\partial C_L}\right)_{\eta} \Big/ \frac{d\eta}{dC_{L_t}}. \tag{3}$$

Ignoring a small term $\frac{m_q}{\mu}$, equivalent to about 0·1 per cent $\bar{c}$ at supersonic speeds, it can be shown that $-\left(\frac{\partial C_M}{\partial C_L}\right)_{\eta} = H_m$, the manoeuvre margin. In Ref. 10 the manoeuvre margin was calculated from the frequency of the longitudinal short-period oscillation and an estimated value of the moment of inertia in pitch. The pitching moment of inertia has since been measured on a specially designed ground rig. Analysis of the results of these tests, which are reported in Ref. 11, indicates that the measured value is about 7 per cent greater than the estimated pitching moment of inertia and the manoeuvre margin for 38 000 ft, shown in Fig. 14, has been evaluated using the measured moment of inertia. Hence the elevator pitching power has been deduced, using $\frac{d\eta}{dC_{L_t}}$ measured in the present tests, together with the corrected manoeuvre margin derived from Ref. 10. The elevator pitching power, shown in Fig. 15 reaches a peak value at $M = 0{\cdot}9$, and falls at supersonic speeds.

It is possible to derive the lifting power of the elevators, $\left(\frac{\partial C_L}{\partial \eta}\right)_{\alpha}$, from the difference between the trimmed and untrimmed lift-curve slopes, $\frac{dC_{L_t}}{d\alpha}$ and $\left(\frac{\partial C_L}{\partial \alpha}\right)_{\eta}$, respectively. They can be shown to be related by the equation

$$\frac{dC_{L_t}}{d\alpha} = \left(\frac{\partial C_L}{\partial \alpha}\right)_\eta + \left(\frac{\partial C_L}{\partial \eta}\right)_\alpha \left(\frac{d\eta}{dC_{L_t}}\right)\left(\frac{dC_{L_t}}{d\alpha}\right) \tag{4}$$

and thus the elevator lifting power is

$$\left(\frac{\partial C_L}{\partial \eta}\right)_\alpha = \left\{\frac{dC_{L_t}}{d\alpha} - \left(\frac{\partial C_L}{\partial \alpha}\right)_\eta\right\} \Big/ \left(\frac{d\eta}{dC_{L_t}}\right)\left(\frac{dC_{L_t}}{d\alpha}\right). \tag{5}$$

Both the trimmed lift curve slope, $\frac{dC_{L_t}}{d\alpha}$, and $\frac{d\eta}{dC_{L_t}}$ are measured in the present tests. The untrimmed lift curve slope, $\left(\frac{\partial C_L}{\partial \alpha}\right)_\eta$, shown in Fig. 16 was obtained in previous flight tests[10]. The accuracy of the elevator lifting-power measurements, which are shown in Fig. 17, is not very high, since they are determined from the difference between the trimmed and untrimmed lift-curve slopes which are similar in magnitude.

5.4. *Drag.*

Fig. 18 shows the variation of the trimmed drag coefficient with $C_{L_t}^2$ at various Mach numbers from 0·7 to 1·6. As for the lift and trim results, lines have only been drawn through the points at 40 000 ft as there is unsufficient data at the lower altitudes. At subsonic speeds, it is shown in the Appendix, following the analysis of Ref. 12, that the trim drag coefficient should be of the form

$$C_D = P + Q\,C_{L_t} + R\,C_{L_t}^2 \tag{6}$$

where P, Q and R are constants at a given Mach number. The term in C_{L_t} arises because the drag is not a minimum at zero lift. The least-squares method has been used to define a quadratic curve through the subsonic results, and a straight line through the supersonic results as the Appendix shows that the term in C_{L_t} is negligible for the present tests at 40 000 ft.

The results from the lower altitude tests show that at supersonic speeds, the drag above zero lift is greater than at 40 000 ft; this is probably due to the increased elevator angle to trim noted in Fig. 11.

The Appendix shows that at subsonic speeds it is possible to derive C_{D_m}, the minimum drag coefficient, K_1, the induced-drag factor and K_2, the control drag factor, from P, Q and R, providing a value of C_{L_m} is known from wind-tunnel tests. Taking into account the likely errors of the measured data and the assumed value of C_{L_m}, Table 6 shows that the accuracy for C_{D_m} should be ± 5 per cent, for K_1 ± 30 per cent and for K_2 ± 180 per cent. Clearly the method will not give reliable results for K_2, but should give an indication of K_1 and a reasonably reliable value of C_{D_m}.

The Appendix also shows that at appropriate speeds C_{D_m} may be derived, and also K_1 providing that a wind-tunnel value of K_2 is known*. Table 7 shows that at supersonic speeds the error in C_{D_m} is similar to that at subsonic speeds, namely ± 5 per cent, but the error in K_1 is significantly lower.

Figs. 19 and 20 show the variation of the minimum drag coefficient, C_{D_m}, and the induced-drag factor K_1 with Mach number. These data have been derived from the smoothed curves of Fig. 18. The values at Mach numbers of 0·7, 0·97 and 1·00 were not consistent with the remaining points and have not been included. The reason for these inconsistencies at the first two Mach numbers is probably that the lack of data at low lift coefficients makes an accurate definition of the curve impossible. The reason for the inconsistency at $M = 1{\cdot}0$ is not so clear, as in this case there is sufficient data. It may have been caused by the form of the equation assumed for the control drag, equation (9) of the Appendix, which was based on

*The control drag factor, K_2, may be derived from flight test results at two centre of gravity positions. This was attempted in the present tests, but unfortunately due to a curtailment of the tests, insufficient results were obtained to give a reliable value of K_2. Nevertheless it is believed that the flight test technique is capable of giving reliable values of K_2.

low-speed tunnel tests and probably does not apply at so high a speed.

The minimum drag coefficient, C_{D_m}, increases from 0·0130 at subsonic speeds to 0·0198 at supersonic speeds. A major part of this increase is due to wave drag, but the changes of jet interference effects, skin friction and roughness drag may be significant as may be the change in base drag due to the moveable eyelids in the jet pipe.

Fig. 20 compares the measured value with the theoretical minimum, $\frac{1}{\pi A}$, and maximum, $1 \Big/ \left(\frac{\partial C_L}{\partial \alpha}\right)_\eta$, values of K_1, assuming full and zero leading-edge suction is attained respectively. The maximum value is based on the flight measurements of $\left(\frac{\partial C_L}{\partial \alpha}\right)_\eta$, Fig. 16. The accuracy of the measurements is, as expected, not good at subsonic speeds, but the results show that subsonic speeds a significant leading-edge suction force is being attained whereas at supersonic speeds little, if any, is being achieved. This is supported by earlier flight test results[13], where limited pressure measurements at one spanwise station of the wing showed that the leading-edge suction force decreases with increasing Mach number. The reduction in the leading-edge suction force at supersonic speeds is more rapid than theory predicts. The theoretical leading-edge suction force only becomes zero for a 60° delta wing when the leading edge becomes sonic at $M = 2{\cdot}0$.

5.5. *Rear Fuselage Pressures.*

These measurements were made mainly for comparison purposes with wind-tunnel tests[2], since the pressure distribution on the rear fuselage has a very significant effect on the aircraft drag. Rear fuselage pressures measured in flight and tunnel are likely to be different for two reasons. The geometry of the aft end of the wind-tunnel model is slightly different from that of the aircraft and the effect of the jet efflux on these pressures may be significantly different in flight and tunnel since in the tunnel the engine is not represented and the model is mounted on an aft sting.

Fig. 21 shows the pressures measured along the two generators at ± 37° to the centreline plane at Mach numbers from 0·94 to 1·6. These limited results suggest that the pressure distribution is reasonably axisymmetric. There is a marked decrease in the pressures between $M = 0{\cdot}94$ and 1·00 which could possibly be due to a rearward shock movement. With increasing supersonic Mach numbers there is a tendency for the pressures to increase slowly. Most of the measurements were made with the airbrakes free to float; tests with the airbrakes locked showed no significant effect on the measured pressures.

6. *Comparison with Wind-Tunnel Results.*

Wind-tunnel results are available for comparison with flight results from tests on a 1/24 scale model[3,4] and a 1/9 scale model[1,2].

No drag measurements were made on the 1/24 scale model. Although drag measurements have been made on the 1/9 scale model, comparisons with the flight results are not attempted because of the significant differences between the flight and tunnel techniques mentioned in the introduction.

Thus this Section concentrates on a comparison of trim and lift data; because the larger scale model was more representative of the aircraft more detailed comparisons have been made in this case. The most convenient way to make the comparisons is in the form of elevator angle *versus* incidence for the trim data, and trimmed lift coefficient *versus* incidence. In the case of the lift data two comparisons are possible, based on tunnel and flight values of the elevator angle to trim respectively.

Fig. 22 shows a comparison of the elevator angle to trim measured in flight and tunnel tests. The agreement between A.R.A.[1] and R.A.E.[2] results on the 1/9 scale model, although limited to only two Mach numbers, is good. In the case of the flight and tunnel results the agreement for the slopes of the trim curves is, in general, quite good, but there are some differences due to differences in C_{m_0}. One of the major reasons for differences between flight and tunnel values of C_{m_0} must be caused by differences in the aileron rigged-up angle, in the tunnel this was 2·9°, whereas in flight Fig. 12 shows that it has a value of approximately 3·8° for most flight condition, but can increase to about 4·1° at $M = 1{\cdot}65$. The trim curves (Fig. 22) at $M = 0{\cdot}7$ and 0·8 show only small differences between flight and tunnel in spite of the different settings

of the aileron rigged-up angle. This may be because of the different type of loading due to control deflection at subsonic and supersonic speeds causing lower pitching-moment increments at subsonic speeds, or to some other aerodynamic effect occurring which counterbalances the effect of the different aileron settings.

At transonic speeds, $M = 0{\cdot}9$ to $1{\cdot}0$ the differences in elevator angle to trim are quite large amounting to almost 2°. This probably reflects the difficulty of representing the flow correctly in the tunnel at transonic speeds and there is probably a fundamental difference in elevator pitching power between tunnel and flight in this region. At higher speeds the flight values of the elevator angle to trim gradually become less negative compared with the tunnel values reflecting the increase in aileron rigged-up angle measured in flight, Fig. 12.

Figs. 23 and 24 show comparisons of flight and tunnel lift data, the tunnel trimmed-lift values being based on flight and tunnel values of the elevator angle to trim respectively. The agreement between A.R.A. and R.A.E. tunnel results is, as in the case of trim data, good.

Fig. 23 shows in some cases differences between flight and tunnel results which appear to be consistent with the trim data of Fig. 22, but cannot be explained solely in terms of the differences in aileron rigged-up angle. Fig. 24 shows that when both the elevator and aileron pitching moments are effectively included in the trim geometry, agreement between flight and tunnel is somewhat better but differences still exist.

Some derivatives from tunnel tests[1,2,3,4] have also been compared with flight values, both from the present and previous tests.

Figs. 10 and 16 compare values of the trimmed and untrimmed lift-curve slope respectively. Except at transonic speeds the agreement is quite good.

Fig. 15 compares values of the elevator pitching power, and agreement, except at transonic speeds is reasonably good. This may be fortuitous since the flight values of $\left(\frac{\partial C_M}{\partial \eta}\right)_{C_L}$ were derived using measured values of the manoeuvre margin H_m (equation (3)). It is seen from Fig. 14 that the agreement between tunnel and flight values of the manoeuvre margin is poor. The individual tunnel results agree quite well but the increase in manoeuvre margin from subsonic to supersonic speeds is very significantly smaller in flight. A different aerodynamic-centre position is implied between flight and tunnel.

Earlier tunnel and flight work on the aircraft[14] has shown that the development of the wing upper-surface vortices is different between flight and tunnel. This different development would be very likely to lead to different aerodynamic-centre positions while possibly not affecting the lift slopes significantly.

Fig. 17 compares tunnel and flight values of the elevator lifting power; the agreement is only fair but the accuracy of the flight results is not expected to be good (Section 5.3).

7. *Conclusions.*

The lift, longitudinal trim and drag of the Fairey Delta 2 have been measured up to a Mach number of 1·65 at 40 000 ft; some limited tests have also been made at lower altitudes to investigate the magnitude of aeroelastic effects. Most of the tests were made under non-stabilised conditions, but consistent results have been obtained. Comparisons have been made with lift and trim data measured on 1/24 and 1/9 scale wind-tunnel models.

The effect of altitude on the flight results for lift is small, but is significant for the elevator angle to trim even after correcting for elevator distortion. This effect is probably due to changes in aileron rigged-up angle and changes in pressure distribution due to Reynolds number effects.

At subsonic speeds the drag is not a linear function of $C_{L_t}^2$, the trimmed lift coefficient, but includes a term proportional to C_{L_t} which arises becauses the drag is not a minimum at zero lift. At supersonic speeds this term is negligible. A reduction in altitude causes an increase in C_D for a given M and C_{L_t}; this is probably due to the increased up elevator angle required to trim at lower altitudes. The minimum drag coefficient C_{D_m} increases from 0·0130 at subsonic speeds to 0·0198 at supersonic speeds.

The drag due to lift is close to the theoretical minimum at subsonic speeds showing that a significant leading-edge suction force is developed, but at supersonic speeds is close to the theoretical maximum value of $1 \Big/ \left(\frac{\partial C_L}{\partial \alpha}\right)_\eta$.

Limited pressure measurements on the rear fuselage suggest that the pressure distribution is reasonably axisymmetric and that any airbrake floating movement has no significant effect on the pressures. Between $M = 0{\cdot}94$ and $1{\cdot}00$ a shock wave probably moves aft over the rear fuselage.

A comparison of flight and tunnel results shows good agreement for the slope of the elevator angle to trim curves, but differences of up to 2° in trim can occur. The trimmed lift data also shows some differences which, while appearing consistent with the different elevator angles to trim, cannot be completely explained in terms of the different aileron rigged-up angles in flight and tunnel. It is probable that the lift and pitching moment are affected by the known differences in the development of the upper wing-surface vortex.

Agreement between the flight and tunnel values of the elevator pitching power and trimmed and untrimmed lift-curve slopes is good although that for the elevator pitching power may be fortuitous; agreement for elevator lifting power is fair; the increase in the manoeuvre margin from subsonic to supersonic conditions is significantly smaller in flight.

LIST OF SYMBOLS

a_x	Acceleration along the flight path, positive forwards, gravity units
A	Aspect ratio
A_4	Effective area of the transition pipe, sq in
A_5	Effective area of the propelling nozzle, sq in
C_D	Drag coefficient
C_{D_m}	Minimum drag coefficient with controls undeflected
ΔC_{D_c}	Incremental drag coefficient due to elevator deflection
ΔC_{D_i}	Induced-drag coefficient
ΔC_{D_p}	Incremental drag coefficient due to swinging probe
C_L	Untrimmed coefficient at zero elevator angle
C_{L_m}	Lift coefficient at C_{D_m}
C_{L_t}	Trimmed lift coefficient
$C_{L_{\eta=0}}$	Trimmed lift coefficient at $\eta = 0$
$C_{L_{\alpha=0}}$	Trimmed lift coefficient at $\alpha = 0$
C_m	Pitching-moment coefficient
C_{m_0}	Pitching-moment coefficient when $C_{L_t} = 0$
C_p	Pressure coefficient
D	Aircraft trimmed drag, lb
F_G	Gross thrust, lb
g	Acceleration due to gravity, ft/sec^2
K_1	Induced-drag factor, equation (8)
K_2	Control drag factor, equations (9) and (16)
H_m	Manoeuvre margin
L	Aircraft trimmed lift, lb
M	Mach number
m_q	Damping in pitch derivative
n	Acceleration normal to flight path, gravity units
P_{0_t}	Free stream total pressure, lb/sq ft
P	A constant, equation (15)
Q	A constant, equation (15)
Q_0	Air mass flow entering the engine intake, lb/sec
R	A constant, equation (15)
S	Wing area, sq ft

T_{0_t}	Free-stream total temperature, °K
V	Aircraft true speed, ft/sec
W	Aircraft weight, lb
α	Wing incidence, degrees
α_F	Fuselage datum incidence, degrees
η	Elevator angle, degrees
μ	Aircraft relative density

REFERENCES

No.	Author(s)	Title, etc.
1	D. Morton	Force and moment measurements on a 1/9 scale model Fairey F.D.2 aircraft. Aircraft Research Association Model Test Note M6/2, (1964).
2	T. A. Cook .. .. .. R. W. Hayward	Force measurements on a 1/9 scale model of the Fairey Delta 2 research aircraft at Mach numbers between 0·6 and 1·8. R.A.E. Technical Report 68 294 (1968).
3	D. J. Kettle	8 ft × 6 ft transonic wind tunnel tests on a 1/24 scale model of the Fairey Delta 2 (ER 103). A.R.C. C.P.656, (1962).
4	M. D. Dobson	Wind tunnel tests at supersonic speeds on a model of the Fairey Delta 2. A.R.C. C.P. 672, (1962).
5	R. Rose .. .. F. W. Dee Miss A. E. Acethorpe	The test bed calibration of an Avon R.A. 28 engine under both non-reheat and reheat conditions with comparison of thrust measurements by a swinging probe and various conventional methods. R.A.E. Technical Note Aero 2681 (A.R.C. 24979), (1962).
6	A. A. Woodfield .. .. Ann Cronin Glynis Vorley	Measurements of the performance of a turbo-jet engine with reheat (Rolls Royce 28R Avon) in high speed flight and under simulated conditions in test beds. A.R.C. R. & M. 3538.
7	C. S. Spavins .. .. .. F. W. Dee	Frequency response and cross effect calibrations of some rate gyros and accelerometers with specific reference to dynamic flight experiments. R.A.E. Technical Note Aero 2830 (A.R.C. 24281), (1962).
8	F. W. Dee .. .. .. D. G. Mabey	Wind tunnel calibration of incidence vanes for use on the Fairey Delta 2 (ER 103). R.A.E. Technical Note Aero 2785 (A.R.C. 23611), (1961).
9	O. P. Nicholas .. .. .. F. W. Dee	Unpublished Mintech Report.
10	D. R. Andrews	Measurements in flight of the longitudinal stability derivatives of a 60° delta wing aircraft (Fairey Delta 2). A.R.C. C.P. 639, 1959.
11	C. S. Barnes .. .. .. A. A. Woodfield	Measurement of the moments and product of inertia of the Fairey Delta 2 aircraft. R.A.E. Technical Report 68 160 (A.R.C. 30 973) (1968).

REFERENCES—*continued*

No.	*Author(s)*	*Title, etc.*
12	F. G. Cane J. R. Collingborne	An analysis of some data on lift-dependent drag at supersonic speeds. R.A.E. Technical Note Aero 2424 (A.R.C. 18860), (1955).
13	J. S. Roper	The Fairey Delta 2. Measurement of leading edge pressures in supersonic flight. Fairey Aviation Co. Ltd., Aerodynamics Department Report V.1.
14	F. W. Dee O. P. Nicholas	Flight determination of wing flow patterns and buffet boundaries for the Fairey Delta 2 aircraft at Mach numbers between 0·4 and 1·3, and comparisons with wind tunnel results. A.R.C. R. & M. 3482.

APPENDIX

The Variation of Total-Drag Coefficient with Trimmed Lift Coefficient.

The analysis outlined applies in general to all aircraft. However, the non-linear variation of the drag coefficient with the square of the lift coefficient revealed by the analysis, is only apparent if the elevatorlift is significant, namely for tailless aircraft.

Following Ref. 12, it is assumed that the drag coefficient is of the form

$$C_D = C_{D_m} + \Delta C_{D_i} + \Delta C_{D_c} \tag{7}$$

where C_{D_m} is the minimum drag with controls undeflected*, ΔC_{D_i} is the induced drag due to lift with controls undeflected, and ΔC_{D_c} is the drag due to elevator deflection.

The induced drag is taken as

$$\Delta C_{D_i} = K_1 (C_L - C_{L_m})^2 \tag{8}$$

where C_L = untrimmed lift coefficient at zero elevator angle

C_{L_m} = lift coefficient at C_{D_m} (zero for a symmetrical aircraft)

K_1 = a constant, at a given Mach number.

Subsonic.

Unpublished wind-tunnel tests at low speed on the Fairey Delta 2 suggest that a good approximation of the control drag is given by

$$\Delta C_{D_c} = K_2 (\eta^2 + 4\alpha\eta) \tag{9}$$

where η = elevator deflection

α = wing incidence

K_2 = a constant, at a given Mach number.

Thus, at subsonic speeds, the drag coefficient is assumed to be

$$C_D = C_{D_m} + K_1 (C_L - C_{L_m})^2 + K_2 (\eta^2 + 4\alpha\eta) . \tag{10}$$

As it is wished to express the drag coefficient in terms of the trimmed lift coefficient, we must use the following expressions, which apply if the variation of lift with incidence and control deflection is linear

$$C_L = C_{L_t} - \left(\frac{\partial C_L}{\partial \eta} \right)_\alpha \eta , \tag{11}$$

$$\eta = \frac{d\eta}{dC_{L_t}} (C_{L_t} - C_{L_{\eta=0}}) , \tag{12}$$

$$\alpha = \frac{d\alpha}{dC_{L_t}} (C_{L_t} - C_{L_{\alpha=0}}) , \tag{13}$$

*Ailerons are uprigged 3·2° in the undeflected case for the Fairey Delta 2.

where $C_{L_{\eta=0}}$ = trimmed lift coefficient at $\eta = 0$

$C_{L_{\alpha=0}}$ = trimmed lift coefficient at $\alpha = 0$.

Substituting the expressions (11), (12) and (13) in (10) and re-arranging terms gives,

$$
\begin{aligned}
C_D = C_{D_m} &+ K_1 \left\{ C_{L_m} - \left(\frac{\partial C_L}{\partial \eta}\right)_\alpha \left(\frac{d\eta}{dC_{L_t}}\right) C_{L_{\eta=0}} \right\}^2 \\
&+ K_2 \left\{ \left(\frac{d\eta}{dC_{L_t}}\right)^2 C^2_{L_{\eta=0}} + 4\left(\frac{d\eta}{dC_{L_t}}\right)\left(\frac{d\alpha}{dC_{L_t}}\right) C_{L_{\eta=0}} C_{L_{\alpha=0}} \right\} \\
&- 2C_{L_t} \left\{ K_1 \left[1 - \left(\frac{\partial C_L}{\partial \eta}\right)_\alpha \left(\frac{d\eta}{dC_{L_t}}\right) \right] \left[C_{L_m} - \left(\frac{\partial C_L}{\partial \eta}\right)_\alpha \left(\frac{d\eta}{dC_{L_t}}\right) C_{L_{\eta=0}} \right] \right. \\
&\left. + K_2 \left[\left(\frac{d\eta}{dC_{L_t}}\right) C_{L_{\eta=0}} \left(\frac{d\eta}{dC_{L_t}} + \frac{2d\alpha}{dC_{L_t}}\right) + 2C_{L_{\alpha=0}} \cdot \frac{d\alpha}{dC_{L_t}} \cdot \frac{d\eta}{dC_{L_t}} \right] \right\} \\
&+ C^2_{L_t} \left[K_1 \left\{ 1 - \left(\frac{\partial C_L}{\partial \eta}\right)_\alpha \left(\frac{d\eta}{dC_{L_t}}\right) \right\}^2 + K_2 \left\{ \frac{d\eta}{dC_{L_t}} \left(\frac{d\eta}{dC_{L_t}} + 4\frac{d\alpha}{dC_{L_t}} \right) \right\} \right] \qquad (14)
\end{aligned}
$$

which may be expressed as

$$C_D = P + Q\,C_{L_t} + R\,C^2_{L_t}. \qquad (15)$$

It should be noted that the variation of drag with lift includes a term proportional to C_{L_t} as well as the normal term in $C^2_{L_t}$.

The second term on the right hand side of equation (14) is negligible and may be ignored. The third term is fairly small and hence C_{D_m} does not greatly differ from P.

The values of P, Q and R may be obtained from the experimental results using a least-squares method of analysis assuming a function of the form given by equation (15).

P, Q and R are constants at a given Mach number, and are functions of aerodynamic parameters. The values of these parameters are known from the flight test results. The unknown parameters are C_{D_m}, K_1, K_2 and C_{L_m}; any three of them may be derived from P, Q and R if a value for the fourth is known from some other source.

The least important of these parameters is C_{L_m}, and a reasonably accurate value can be obtained from wind-tunnel tests. In the present tests, the effects of errors in C_{L_m} are shown in Table 6. It is seen that errors in C_{L_m} have an insignificant effect on C_{D_m}, although there is an important effect on K_1 and a very large effect on K_2.

Supersonic.

At supersonic speeds the control-drag term is modified, and using simple flat-plate theory

$$\Delta C_{D_c} = K_2 (\eta^2 + 2\eta\alpha). \qquad (16)$$

The equation expresses the fact that at constant incidence the control drag is a minimum when the control is in the streamwise direction, $\eta = -\alpha$. Unpublished tunnel tests on a Fairey Delta 2 model confirm this approximation, although K_2 has some dependence on incidence as well as Mach number.

For the Fairey Delta 2 the equations may be simplified, as the present tests show that $C_{L_{\eta=0}}$ is small at 40 000 ft. The drag equation at supersonic speeds at 40 000 ft becomes

$$C_D = C_{D_m} + K_1 C_{L_m}^2 - 2C_{L_t}\left[C_{L_m} K_1 \left\{ 1 - \left(\frac{\partial C_L}{\partial \eta}\right)\left(\frac{d\eta}{dC_{L_t}}\right)\right\} + K_2 C_{L_{\alpha=0}} \frac{d\alpha}{dC_{L_t}} \frac{d\eta}{dC_{L_t}} \right]$$

$$+ C_{L_t}^2 \left[K_1 \left\{ 1 - \left(\frac{\partial C_L}{\partial \eta}\right)_\alpha \left(\frac{d\eta}{dC_{L_t}}\right)\right\}^2 + K_2 \left\{ \frac{d\eta}{dC_{L_t}} \left(\frac{d\eta}{dC_{L_t}} + 2\frac{d\alpha}{dC_{L_t}} \right) \right\} \right]. \quad (17)$$

The second and third terms on the right hand side of this equation are small and the equation reduces to

$$C_D = C_{D_m} + C_{L_t}^2 \left[K_1 \left\{ 1 - \left(\frac{\partial C_L}{\partial \eta}\right)_\alpha \left(\frac{d\eta}{dC_{L_t}}\right)\right\}^2 + K_2 \left\{ \frac{d\eta}{dC_{L_t}} \left(\frac{d\eta}{dC_{L_t}} + 2\frac{d\alpha}{dC_{L_t}} \right) \right\} \right] \quad (18)$$

and thus the drag is a linear function of $C_{L_t}^2$. The value of C_{D_m} may be derived from the present experimental results, but the induced and control-drag terms may only be separated using the results of tests at two centre of gravity positions. It is interesting to note that if $2\frac{d\alpha}{dC_{L_t}} > -\frac{d\eta}{dC_{L_t}}$, as it is in the present tests for Mach numbers less than 1·6, the control-drag term is negative and reduces the value of $\frac{dC_D}{dC_{L_t}^2}$. This does not imply that the drag of the elevator is negative, but that the upward deflection of the elevator required to trim the aircraft is closer to the minimum-drag condition than is the control undeflected condition.

The present tests show that for the Fairey Delta 2 at the lower altitudes $C_{L_{\eta=0}}$ is not as small as at 40 000 ft, hence an equation of similar form to equation (15) is applicable.

TABLE 1

Fairey Delta 2—Principal Dimensions.

Wing		
Gross area		360 sq ft
Span		26 ft 10 in
Nominal centreline chord		25 ft
Tip chord		1 ft 10 in
Mean aerodynamic chord		16 ft 9 in
Wing section	4% symmetrical, max t/c at	29·5%C
Leading-edge sweepback		59·92°
Trailing-edge sweepback		0°
Twist		0°
Dihedral		0°
Wing setting, with respect to fuselage datum		+1·5°
Elevator		
Net area (one elevator)		20·18 sq ft
Mean chord		3·69 ft
Angular movement	UP	33°
	DOWN	20°
Aileron		
Net area (one aileron)		16·04 sq ft
Mean chord		2·70 ft
Angular movement (about an uprigged angle of 3·2°)	UP	17°
	DOWN	17°
Weight		
Mean weight at test conditions (1300 lb of fuel used)		13 030 lb
Mean centre of gravity position at test conditions, undercarriage up		163·1 in aft of L.E. of centreline chord
Variation of centre of gravity position due to fuel usage		$\pm\frac{1}{2}$ in
Fuel contents		2450 lb

TABLE 2

Summary of the Number of Projections on the Aircraft Surfaces.

Location	Height or depth of irregularities inches	Number of irregularities per sq ft	Wetted area sq ft	Total number of irregularities
Wing upper surface	0·0010 → 0·0012	248	188	46 600
Wing lower surface	0·0015	58	188	10 900
Fuselage	0·0008 → 0·0013	163	467	76 100
Fin and rudder	0·0008	500	69·8	34 900
Ailerons	0·0008 → 0·0009	277	66·4	18 400
Elevators	0·0012	122	80·8	9900

Total number ≏ 200 000

TABLE 3

Summary of Rivet Head Projections on the Aircraft Surfaces.

Wing (excluding undercarriage doors)	
0·50 inch diameter by 0·0025 inch projection	6850
0·25 inch diameter by 0·0030 inch projection	6850
Main wheel undercarriage doors	
0·25 inch diameter by 0·0025 inch projection	1650
Fuselage	
0·25 inch diameter by 0·002 inch projection	32 700
Fin and rudder	
0·35 inch diameter by 0·001 inch projection	2800
Elevator and ailerons	
0·35 inch diameter by 0·005 inch projection	1460
0·25 inch diameter by 0·003 inch projection	1400

TABLE 4

Key to Panel Diagram (Fig. 4)

P = Port, S = Starboard

1 No. 4 tank, fuel drain valve (P and S)
2 Yaw parachute, electrical connection (P and S)
3 No. 4 tank, water drain, outer (P and S)
4 Blanking plate (P and S)
5 Aileron jack (P and S)
6 Aileron jack hydraulic connections, Desynn transmitter (P and S)
7 No. 3 tank, electrical fuel pump, fuel drain valve in panel (P and S)
8 Hydraulic pipes in trailing edge (P and S)
9 Pressure plotting in elevator (S only)
10 No. 2 tank, fuel drain valve (P and S)
11 No. 2 tank, water drain (P and S)
12 No. 3 tank, water drain (P and S)
13 Accelerometer; Desynn transmitter (P only)
14 Blanking plate (P and S)
15 Main undercarriage door, outer (P and S)
16 Main undercarriage fixed fairing (P and S)
17 Main undercarriage door, rear (P and S)
18 Main undercarriage door, inner (P and S)
19 Flying controls (P and S); Accelerometer (P)
20 Accelerometer; Desynn transmitter (P only)
21 No. 4 tank, water drain, inner (P and S)
22 Blanking plate (P and S)
23 Elevator rocker arm (P and S)
26 Air intake, structure (P and S)
27 Air intake, lower fairing (P and S)
28 Pressure head attachment
29 Radio bay
30 High pressure oxygen valve and changing point
31 Flying controls; air thermometer
32 Air thermometer mounting; flying controls
33 Nose under carriage bay
34 Camera bay
35 Instrument bay
36 Collector tank fuel pump and drain valve
37 Cockpit pressurisation equipment
38 No. 1 tank, fuel and water drains (P and S)
39 Accessories gear box
40 Ground running air intakes; low pressure fuel cock (S)
41 Fuel filter
42 Engine fuel pump govenor
43 Wheel case breather
44 Oil tank level glass
45 Engine, No. 1 zone cooling extractor in panel
46 Engine removal, side tail jacking point (P and S)
47 No. 2 cooling zone extractor (P and S)
48 Reheat attachment (P and S)
49 Cooling duct—spring panel (P and S)

TABLE 4—*continued*

50 Reheat, high pressure fuel connection
51 Reheat ignition
52 Air connection
53 Detachable rear fuselage
54 Aileron hinge point (4); Accelerometer access port
55 Blanking plate (P and S)
56 Aileron jack (P and S)
57 No. 4 tank, fuel filler (P and S)
58 Hydraulic header tank filters
59 Elevator hinge points (4); Accelerometer access (P only)
60 No. 2 tank, fuel filler (P and S)
61 No. 3 tank, fuel filler
62 Blanking plate (P and S)
63 Main undercarriage, hinge point (P and S)
64 No. 1 tank, fuel filler (P and S)
65 Blanking plate (P and S)
66 Air intake, upper fairing, forward (P and S)
67 Air intake, attachments, upper and lower (P and S)
68 Air intake, upper fairing, aft (P and S)
69 Engine mounting (P and S)
70 Engine mounting (P and S)
71 Ground running auxiliary cooling inlet (P and S)
72 Cooling duct (P and S)
73 Compass detector unit
74 Flying controls
75 Rudder pedal hinges
76 Stand-by aerial mounting
77 Hydraulic header tanks
78 Collector tank fuel filler
79 Collector tank
80 Top decking
81 Brake parachute
82 Pressure plotting in aileron (S only)
83 Pressure plotting in aileron (S only)
84 Hinged cabin latch pin emergency release
85 No. 1 system, hydraulic header tank filler
86 No. 2 system, hydraulic tank filler
87 Collector tank
88 Proportioning valves
89 Regulator valve
90 Regulator valve
91 Aircraft air services from compressor
92 Radio mounting
93 External hood jettison
94 Ground pressurising connection
95 Jacking point (P and S)
96 Accelerometer
97 Accelerometer
98 Blanking plate

TABLE 4—*continued*

99 Blanking plate
100 Rudder jack upper trunnion fitting bolts
102 Stand-by radio; oxygen bottle
103 Wind driven emergency hydraulic pump
104 Accelerometer (P only)
105 Accelerometer (P and S)
106 Rudder hinge carrier attachments, upper
107 Rudder hinge carrier attachments, lower

TABLE 5

Data on Unsealed Control Surface Gaps.

			Length of gaps inches	Width of gaps inches
Ailerons	Port	Upper surface	16·5	0·10
		Lower surface	5·0 6·0	0·07 0·10
	Starboard	Upper surface	12·5	0·10
		Lower surface	12·2	0·10
Elevators	Port	Upper surface	15·5	0·15
		Lower surface	6·0 6·0	0·02 0·05
	Starboard	Upper surface	15·9	0·10
		Lower surface	7·7 6·8	0·10 0·07

TABLE 6

Expected Errors in C_{D_m}, K_1 and K_2 at Subsonic Speeds.

Parameter	Expected errors due to errors in:				Expected rms error
	C_L	P	Q	R	
C_{D_m}	$\pm\frac{1}{2}\%$	$\pm 5\%$	$\pm 1\%$	$\pm 1/10\%$	$\pm 5\%$
K_1	$\pm 16\%$	—	$\pm 25\%$	$\pm 4\%$	$\pm 30\%$
K_2	$\pm 100\%$	—	$\pm 150\%$	$\pm 6\%$	$\pm 180\%$

Note: This Table only applies for those subsonic Mach numbers where there is adequate data at low C_L^2 to define the minima of the curves. The errors are very much greater at $M = 0{\cdot}7$ and 0·94 for instance.

TABLE 7

Expected Errors in C_{D_m} and K_1 at Supersonic Speeds.

Parameter	Expected error in K_1 due to errors in:		Expected rms error
	$\frac{dC_D}{dC_{L_t}^2}$	K_2	
K_1	$\pm 3\%$	$\pm 3\%$	$\pm 4{\cdot}2\%$

Expected Errors in C_{D_m} read from curves of Fig. 18 = $\pm 5\%$.

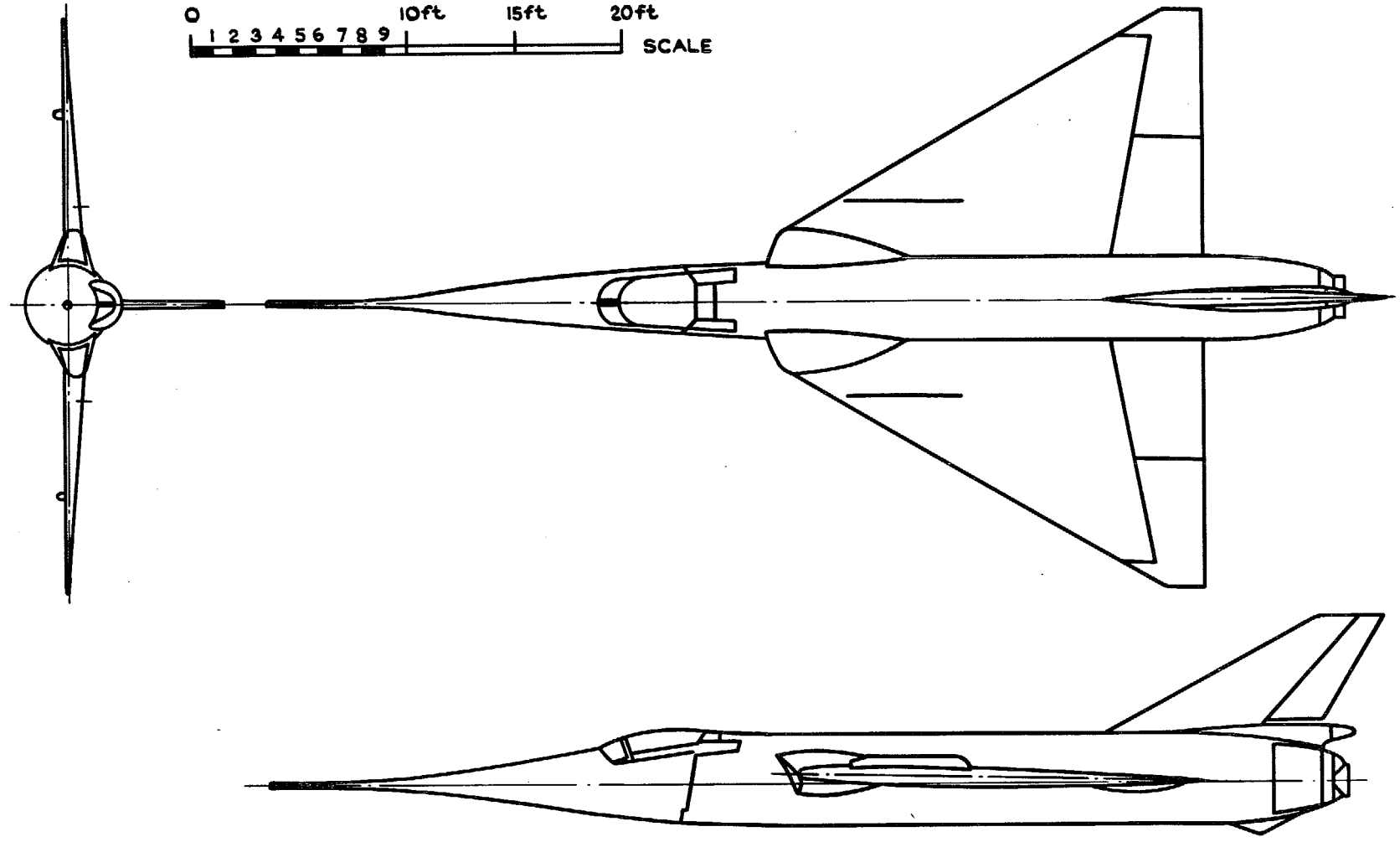

FIG. 1. General arrangement of the Fairey Delta 2.

FIG. 2. The Fairey Delta 2.

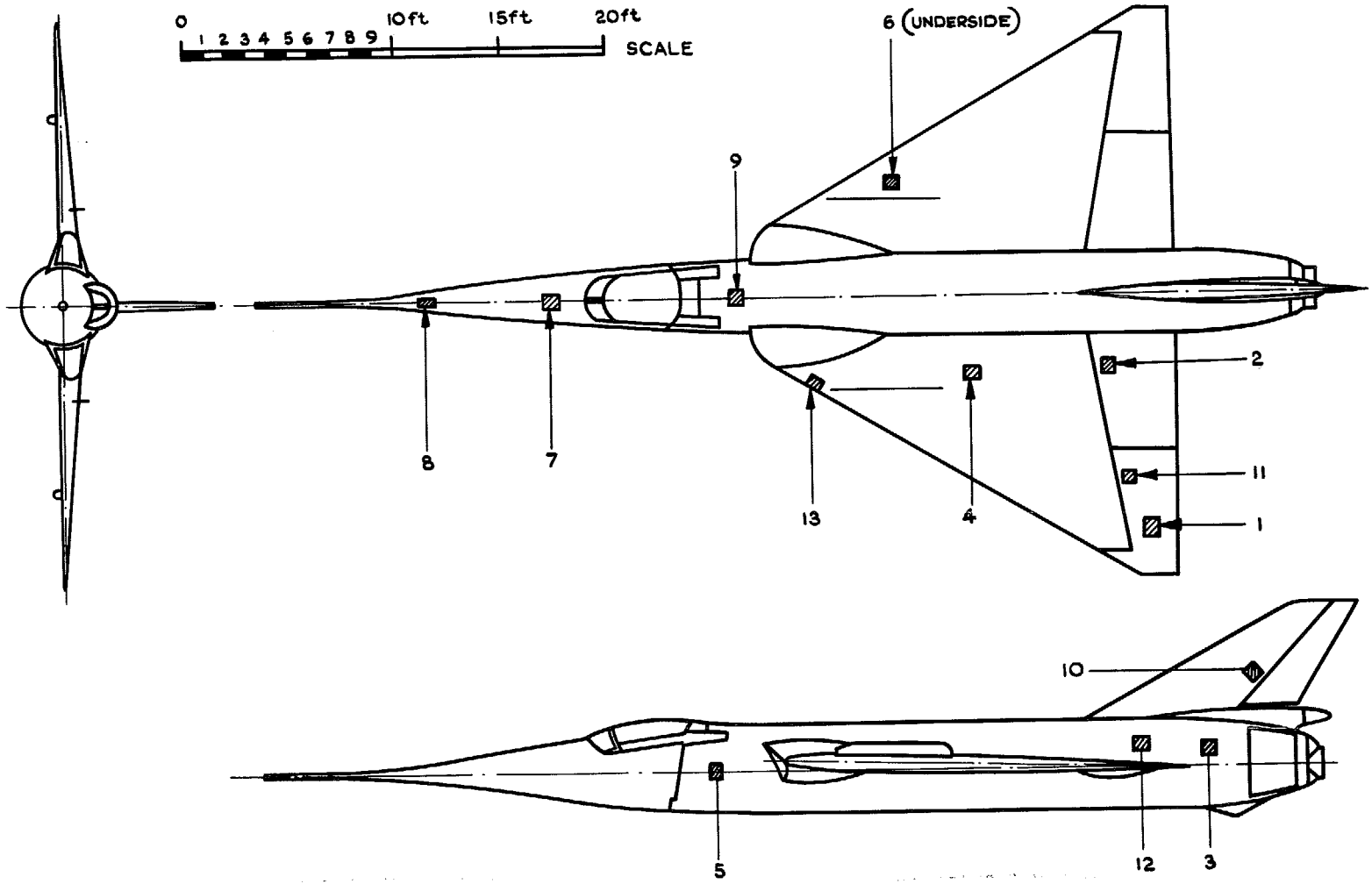

FIG. 3. Position of castings on aircraft surface.

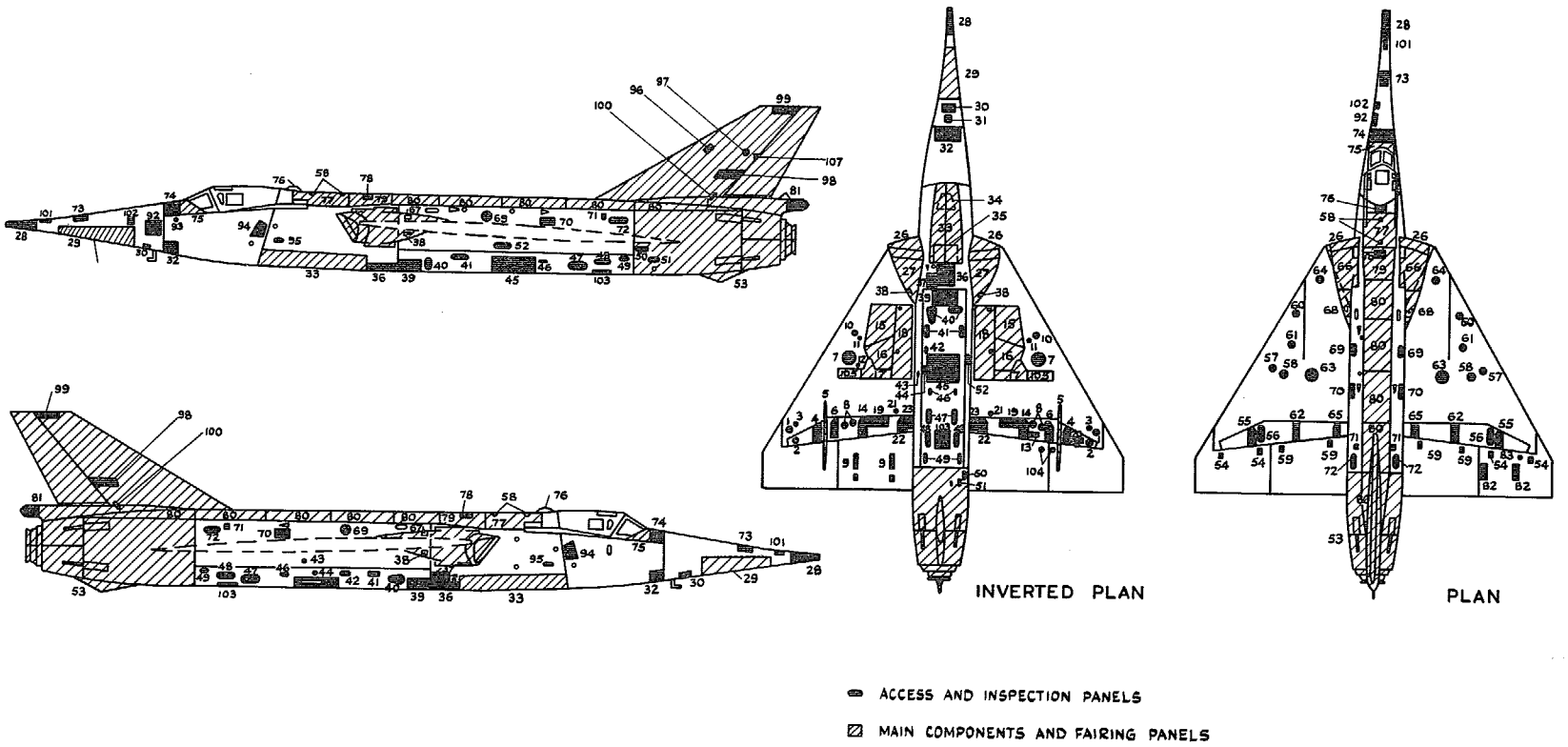

FIG. 4. Positions of access and inspection panels.

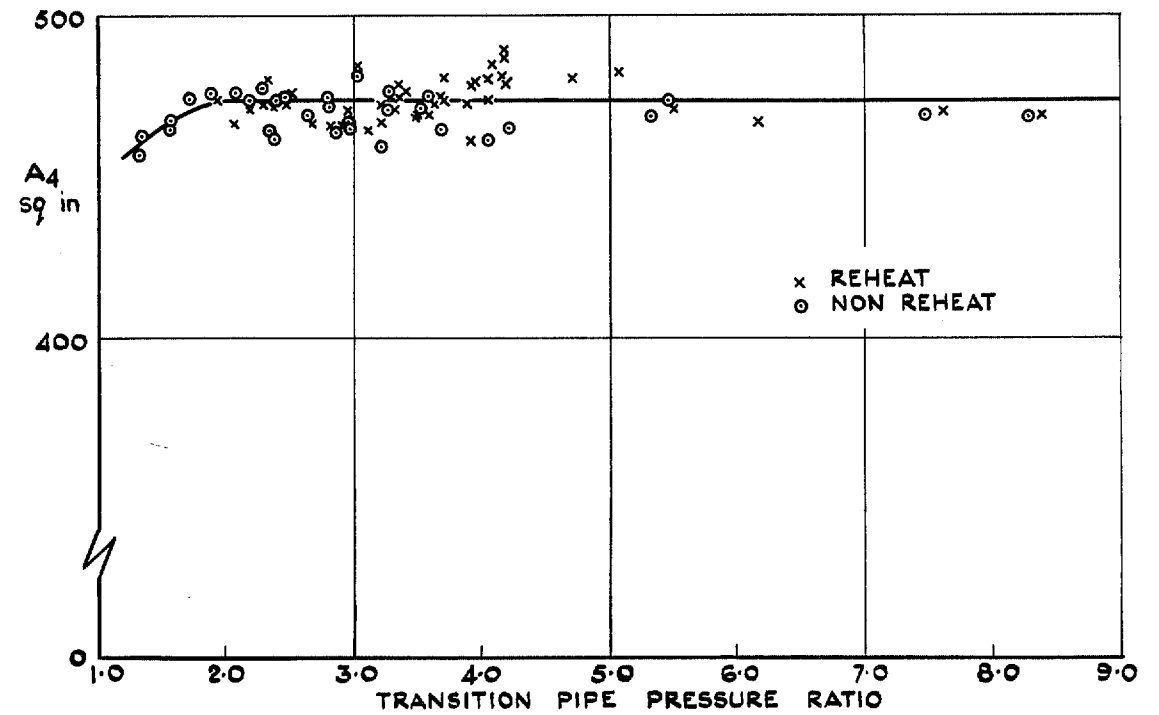

FIG. 5. Effective area of the transition section.

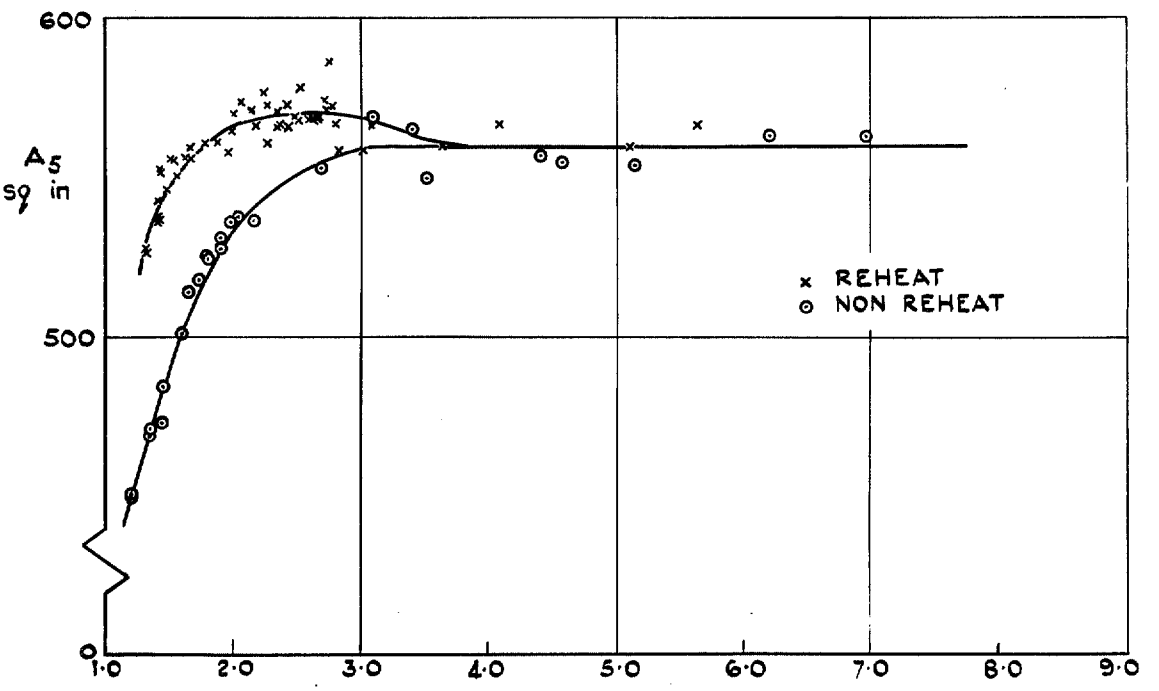

FIG. 6. Effective area of the propelling nozzle.

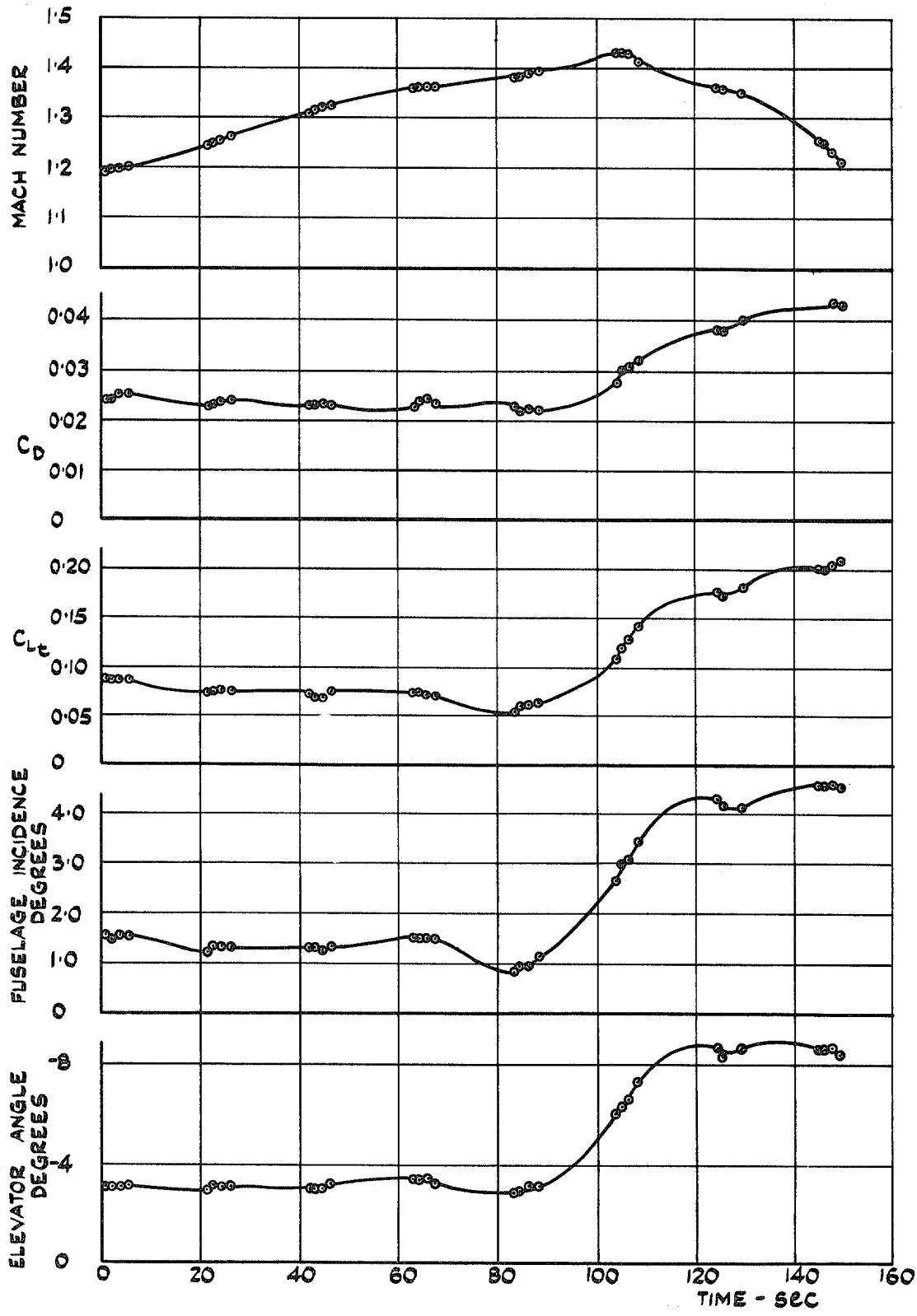

FIG. 7. Time history of typical flight record.

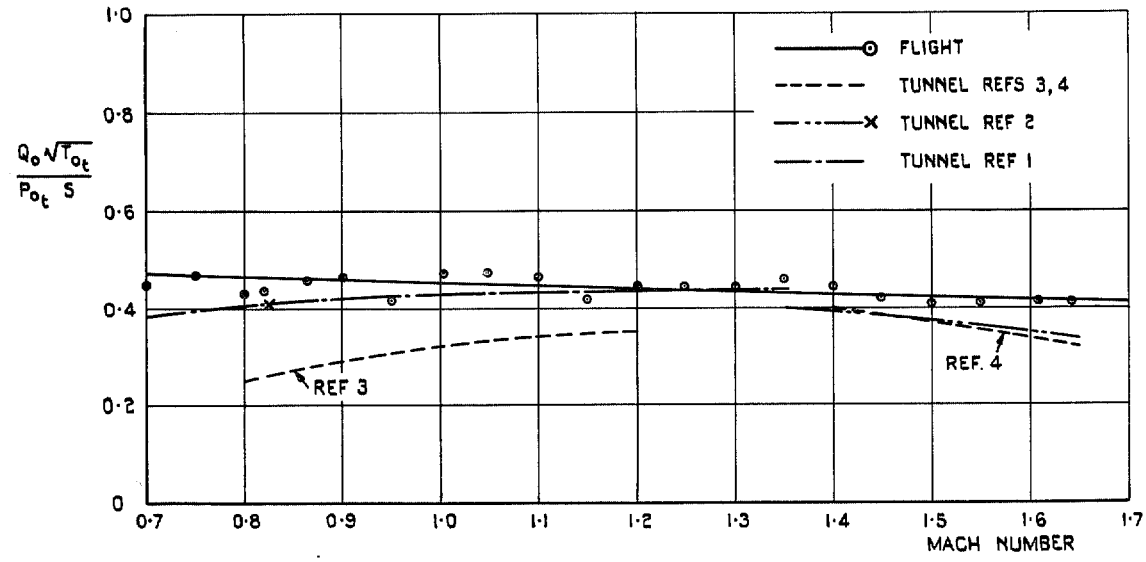

FIG. 8. Non-dimensional engine air mass flow *versus* Mach number.

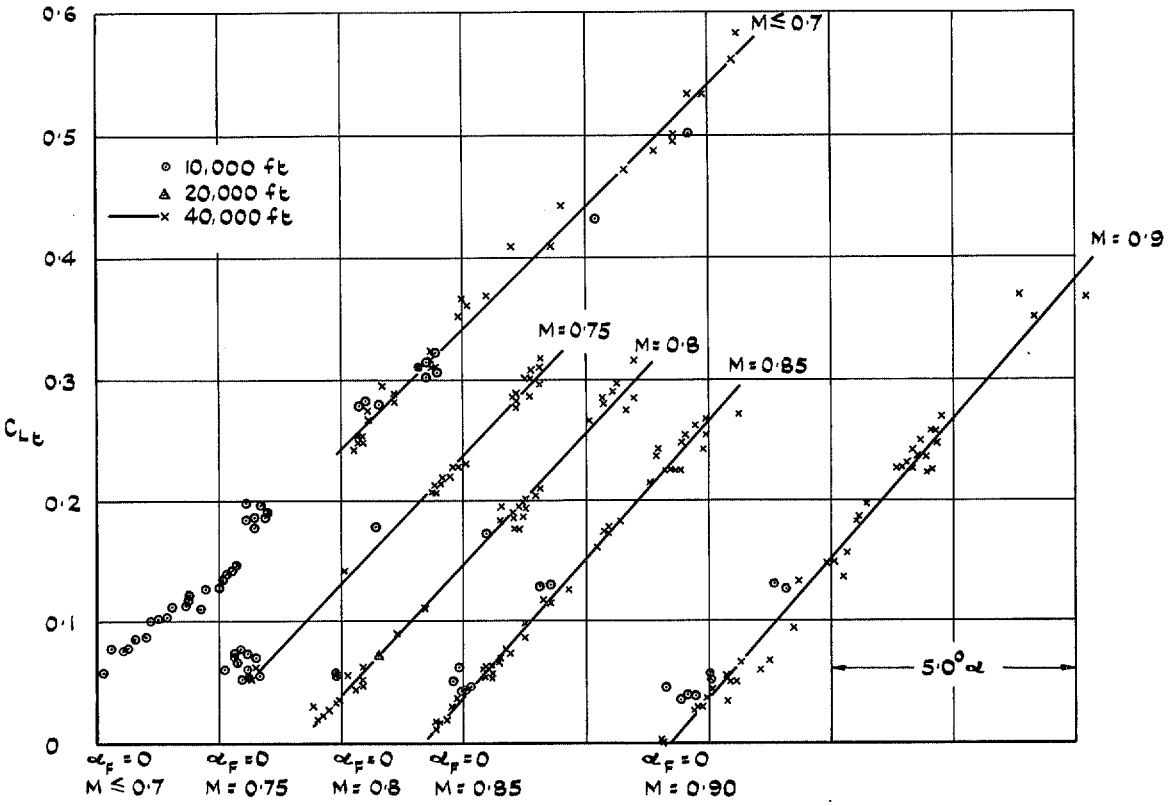

FIG. 9. Variation of trimmed lift coefficient with incidence for various Mach numbers.

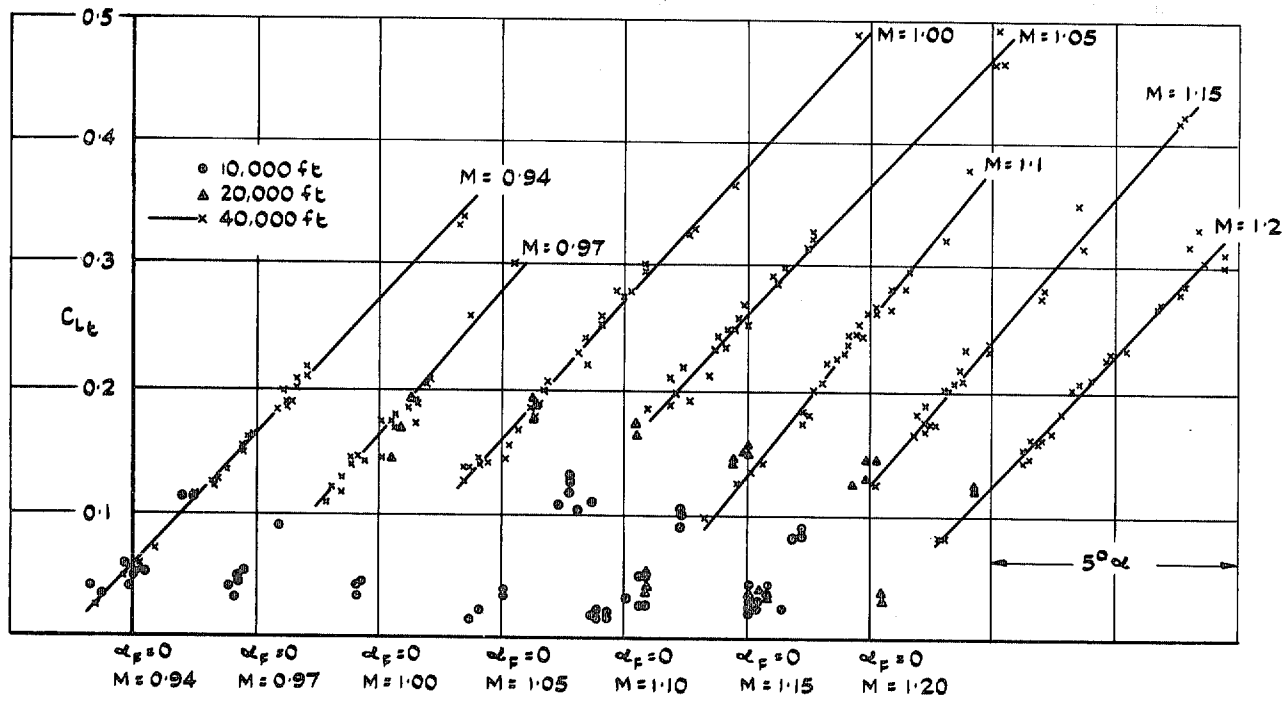

FIG. 9 contd. Variation of trimmed lift coefficient with incidence for various Mach numbers.

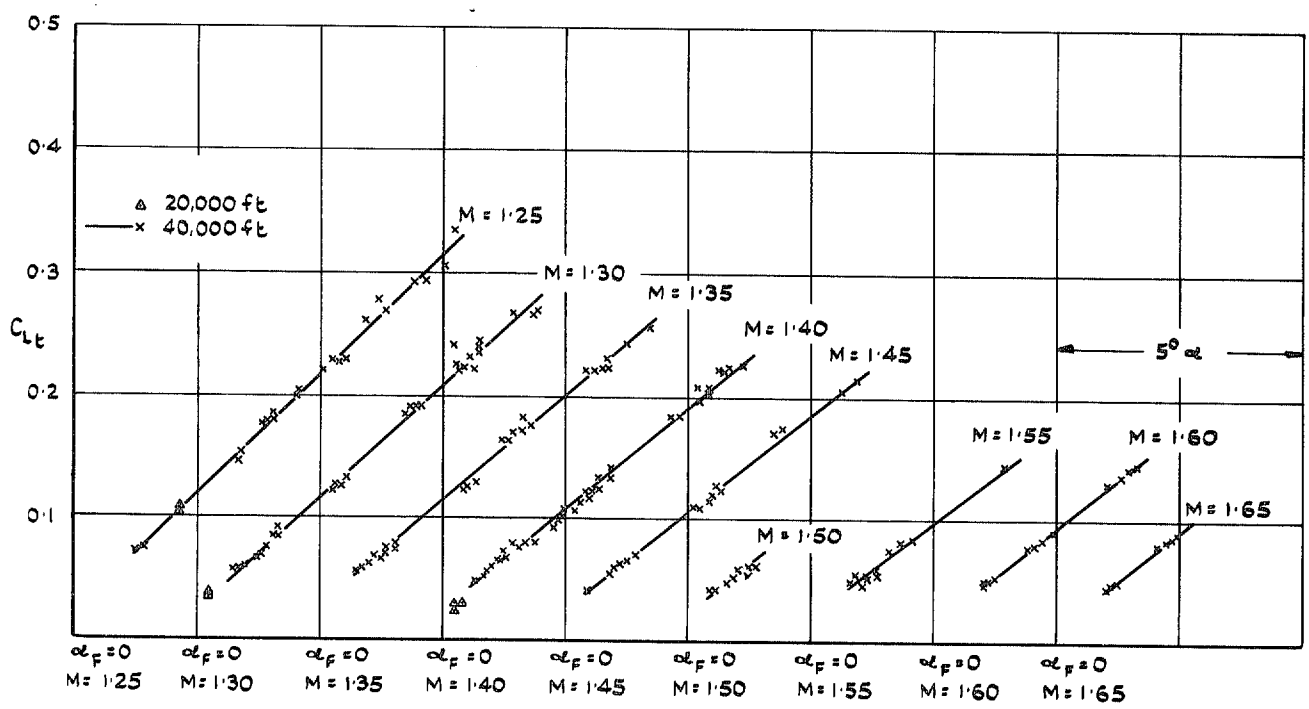

FIG. 9 concld. Variation of trimmed lift coefficient with incidence for various Mach numbers.

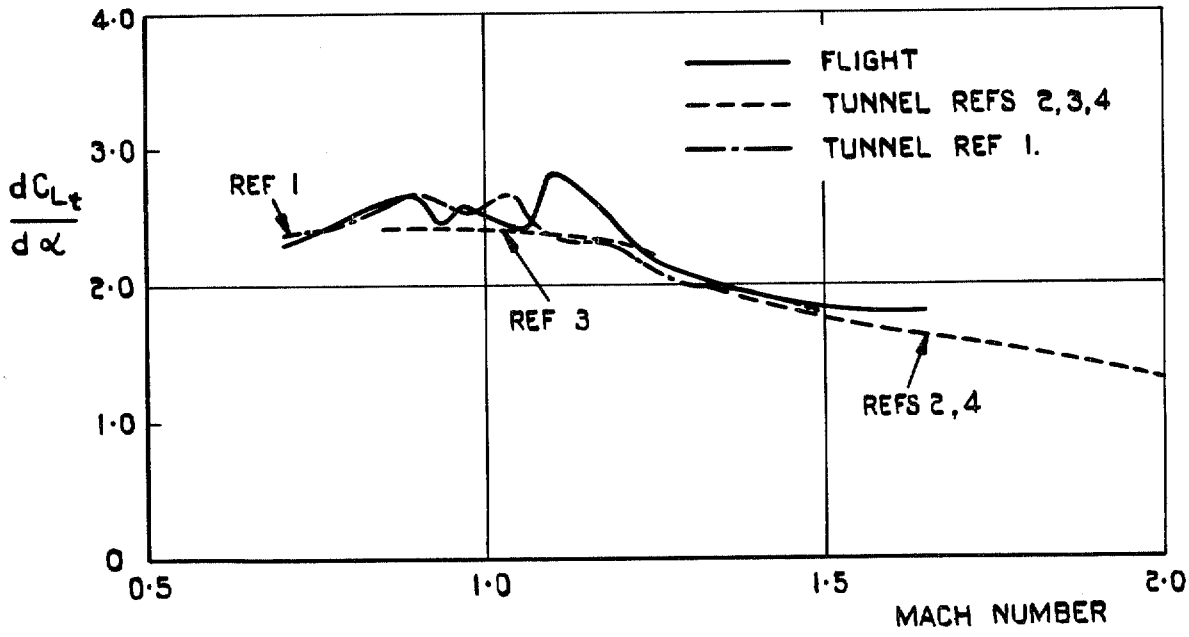

FIG. 10. Variation of trimmed lift curve slope with Mach number.

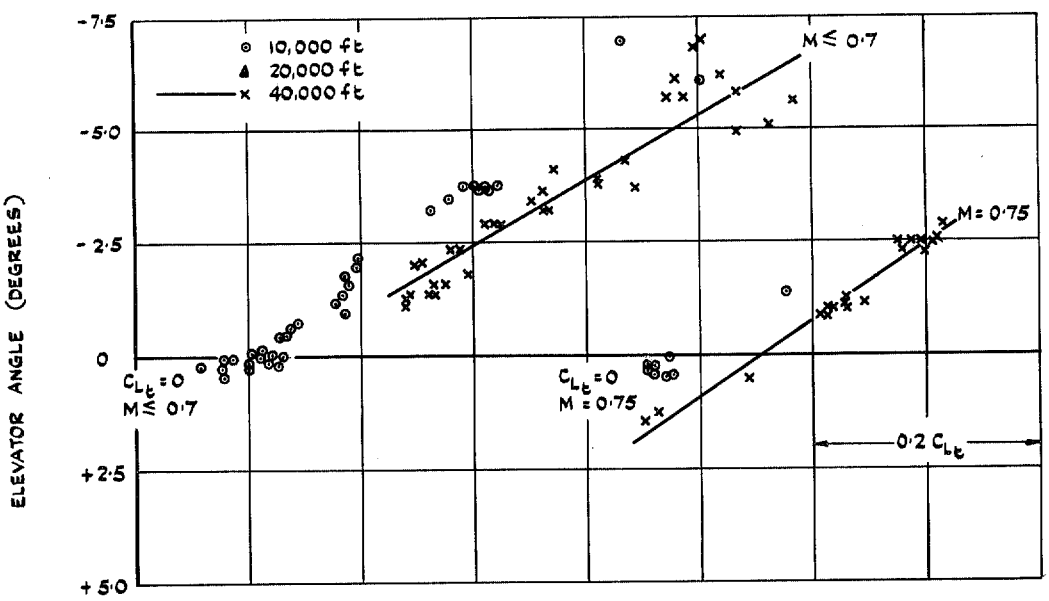

FIG. 11a. Variation of elevator angle with trimmed lift coefficient for various Mach numbers.

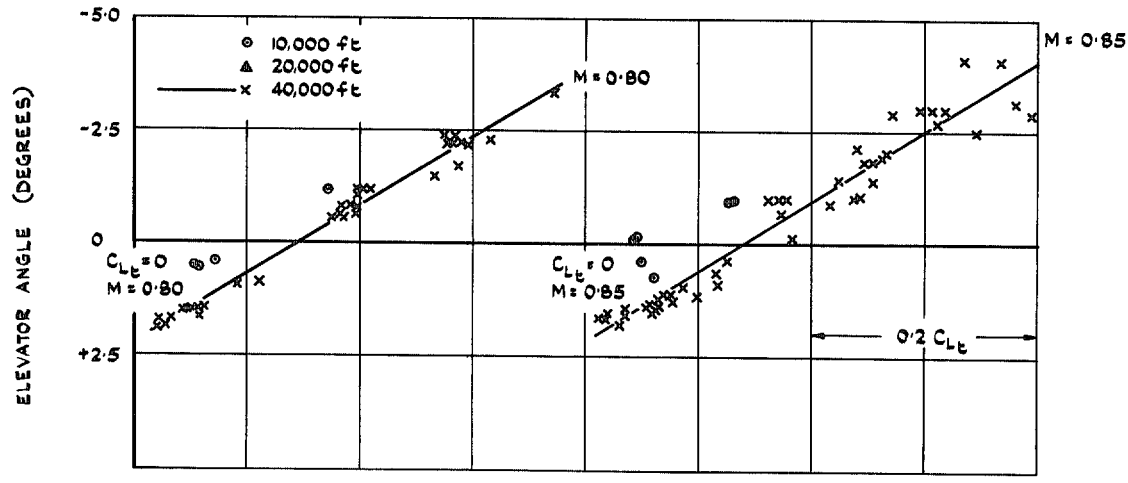

FIG. 11b. Variation of elevator angle with trimmed lift coefficient for various Mach numbers.

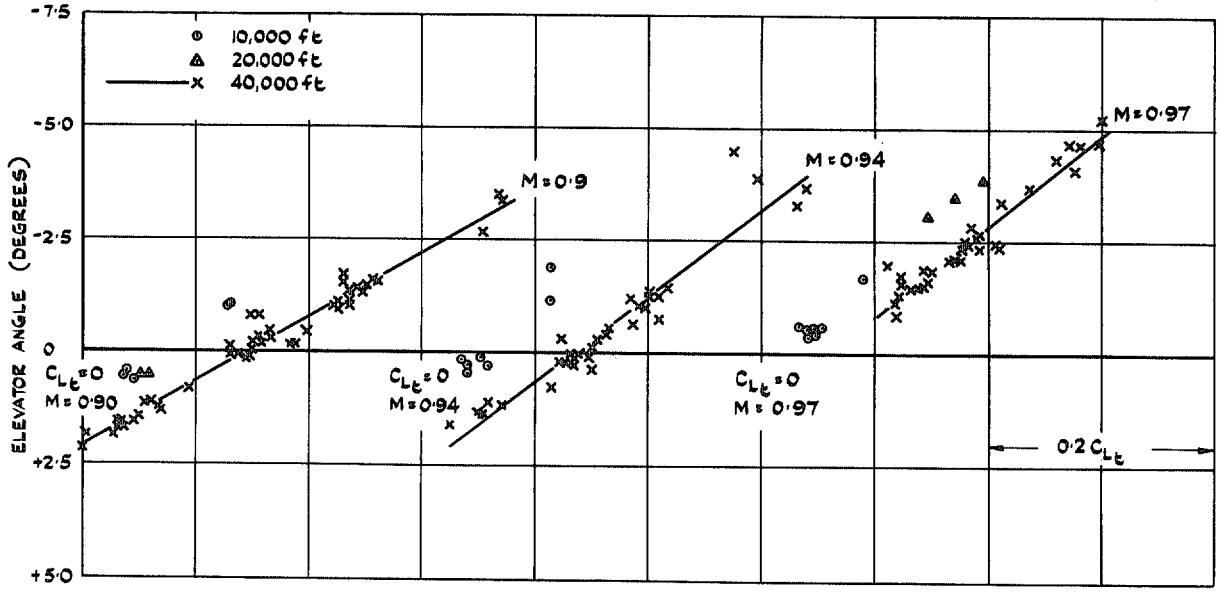

FIG. 11c. Variation of elevator angle with trimmed lift coefficient for various Mach numbers.

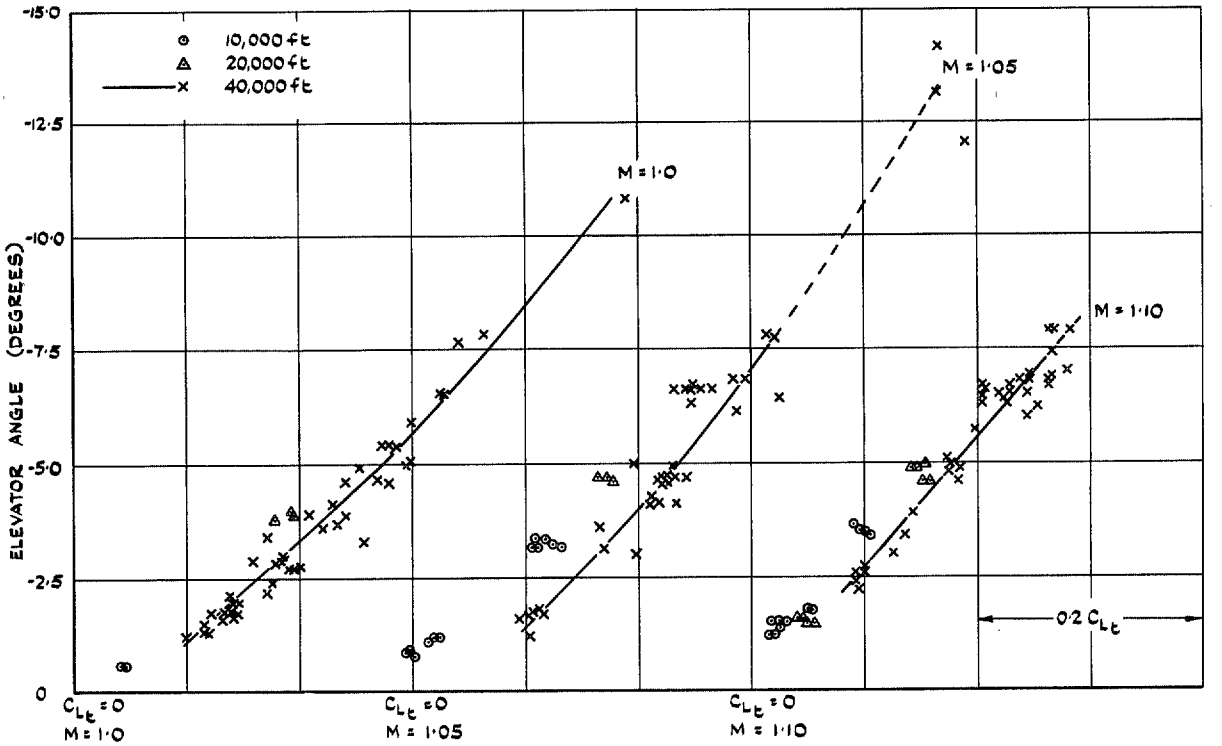

FIG. 11d. Variation of elevator angle with trimmed lift coefficient for various Mach numbers.

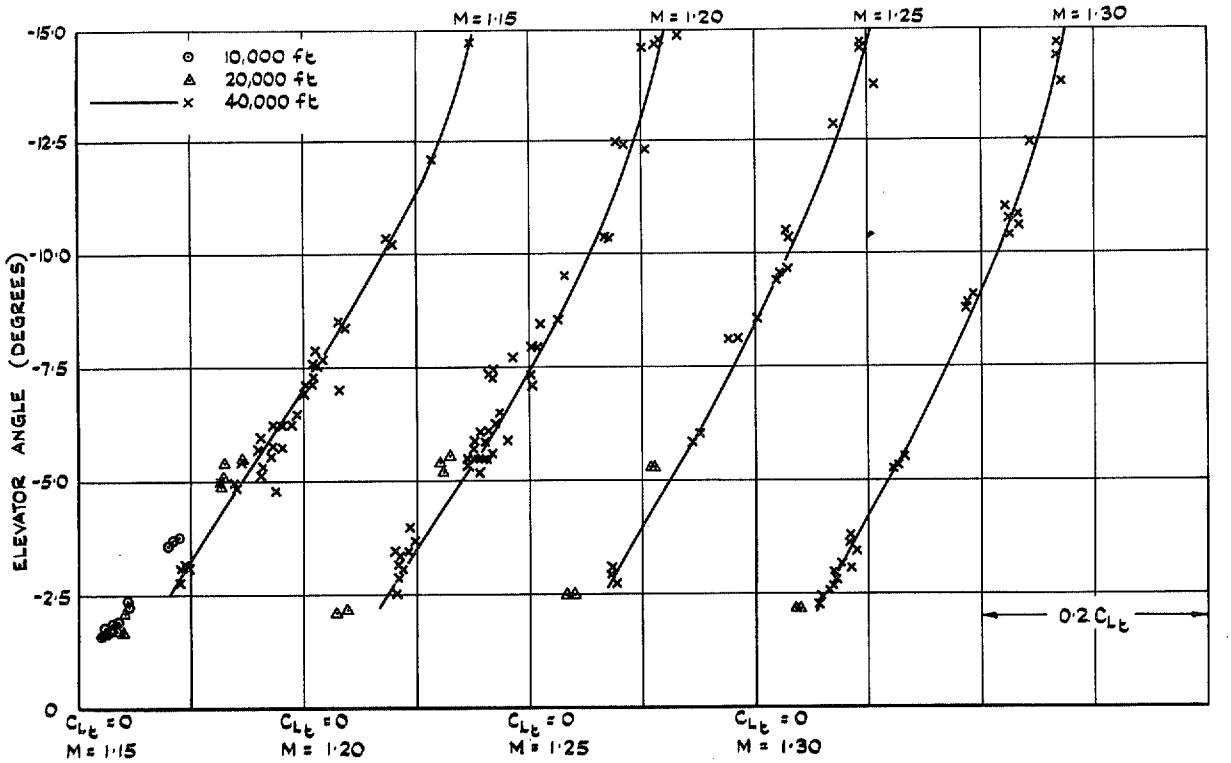

FIG. 11e. Variation of elevator angle with trimmed lift coefficient for various Mach numbers.

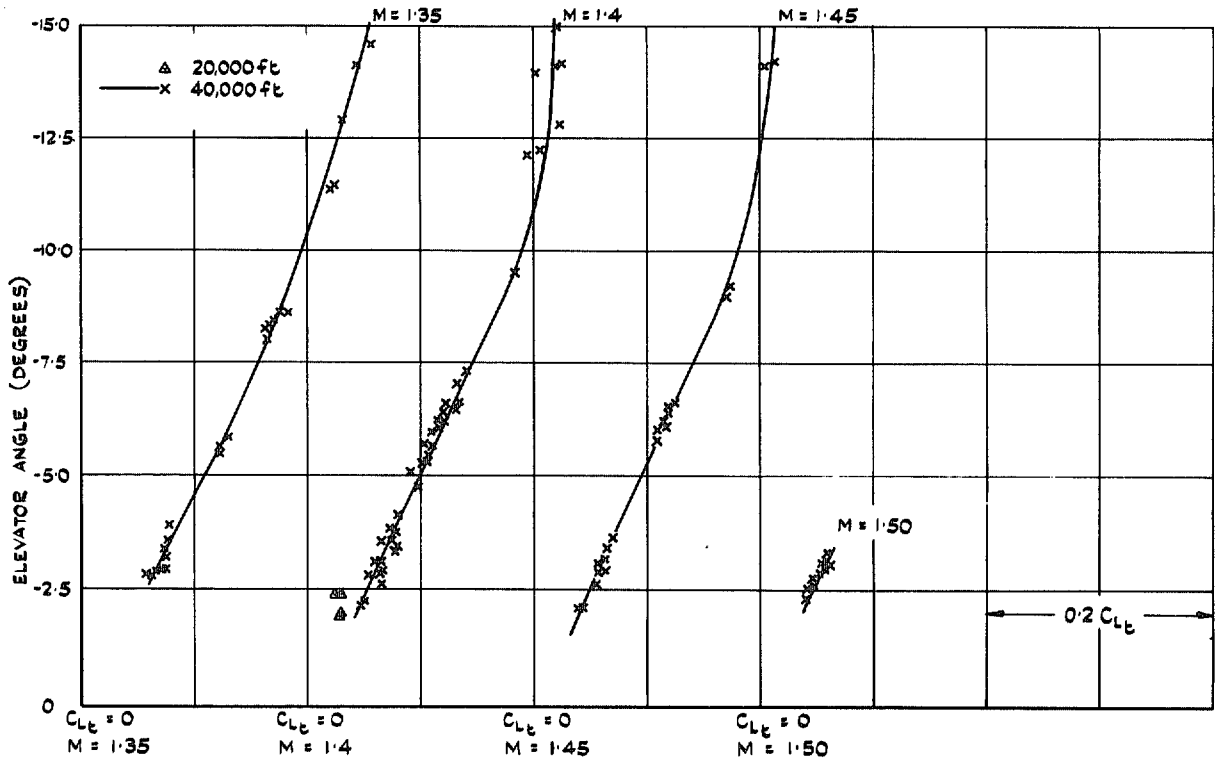

FIG. 11f. Variation of elevator angle with trimmed lift coefficient for various Mach numbers.

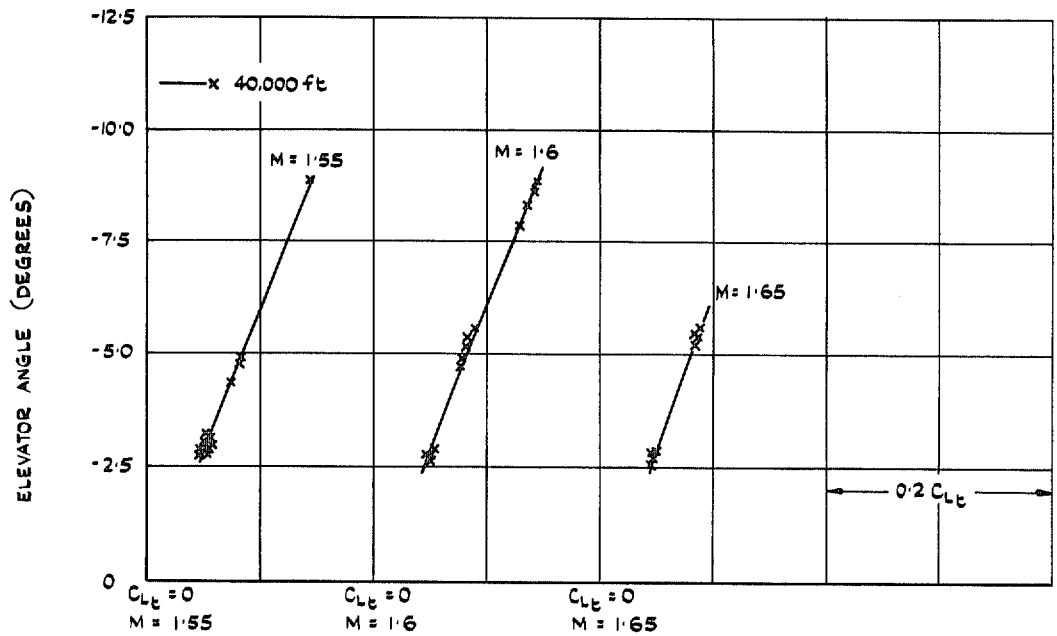

FIG. 11g. Variation of elevator angle with trimmed lift coefficient for various Mach numbers.

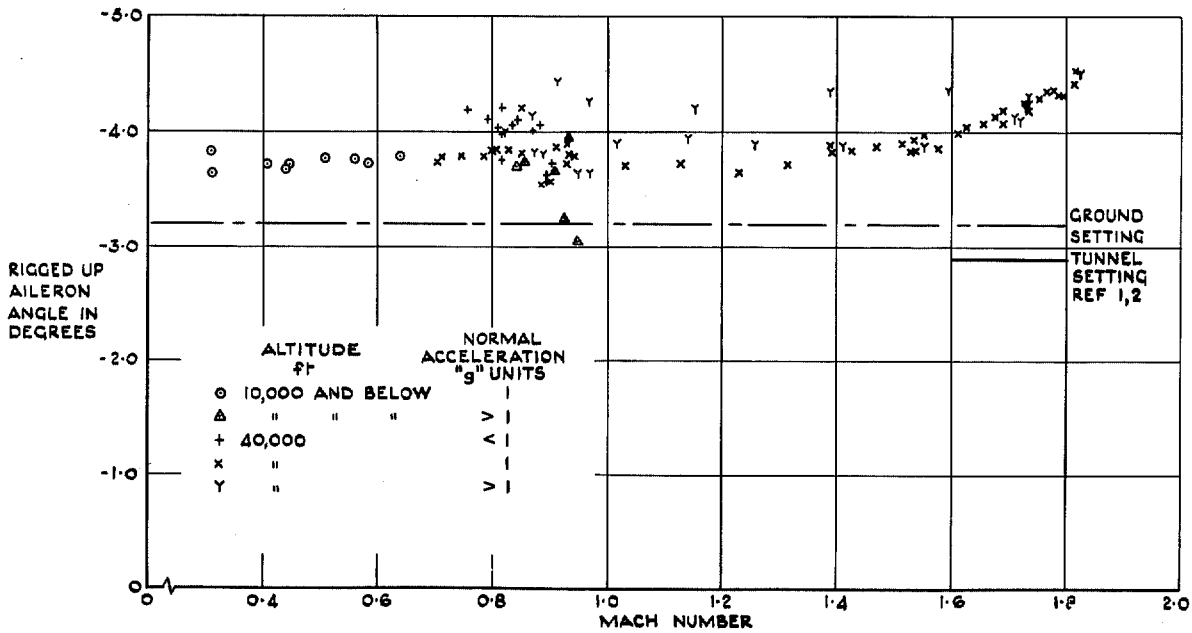

FIG. 12. Measured aileron rigged-up angle in flight.

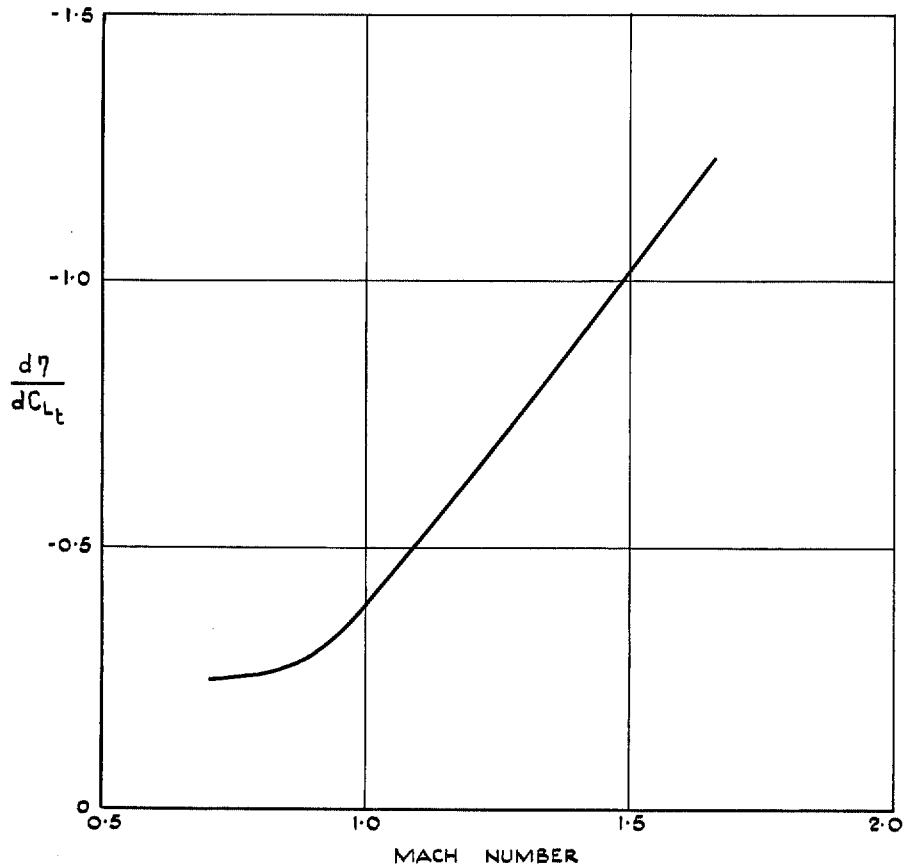

FIG. 13. Variation of $\frac{d\eta}{dC_{L_t}}$ with Mach number (40 000 ft).

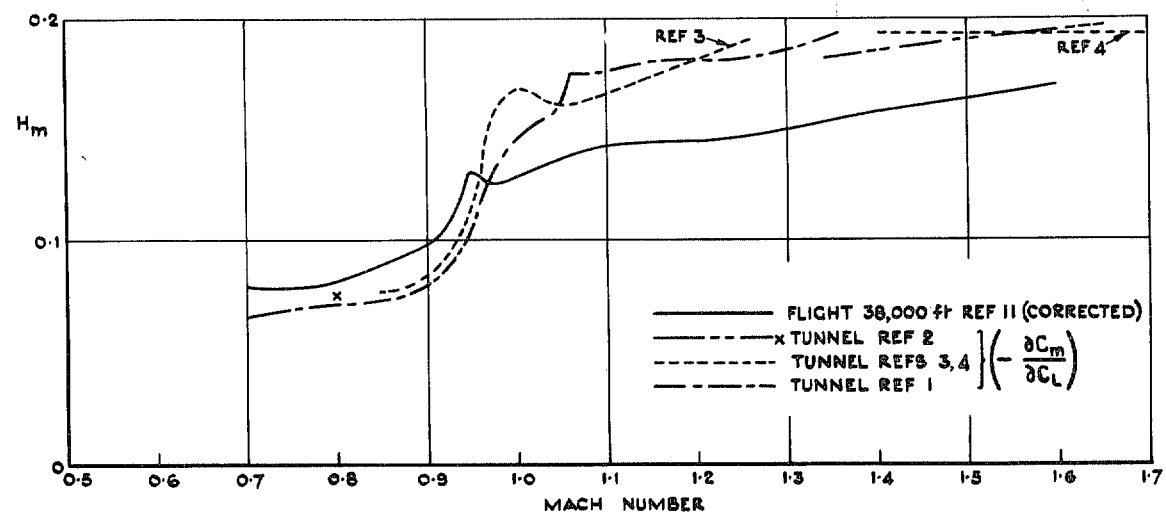

FIG. 14. Variation of manoeuvre margin H_m with Mach number.

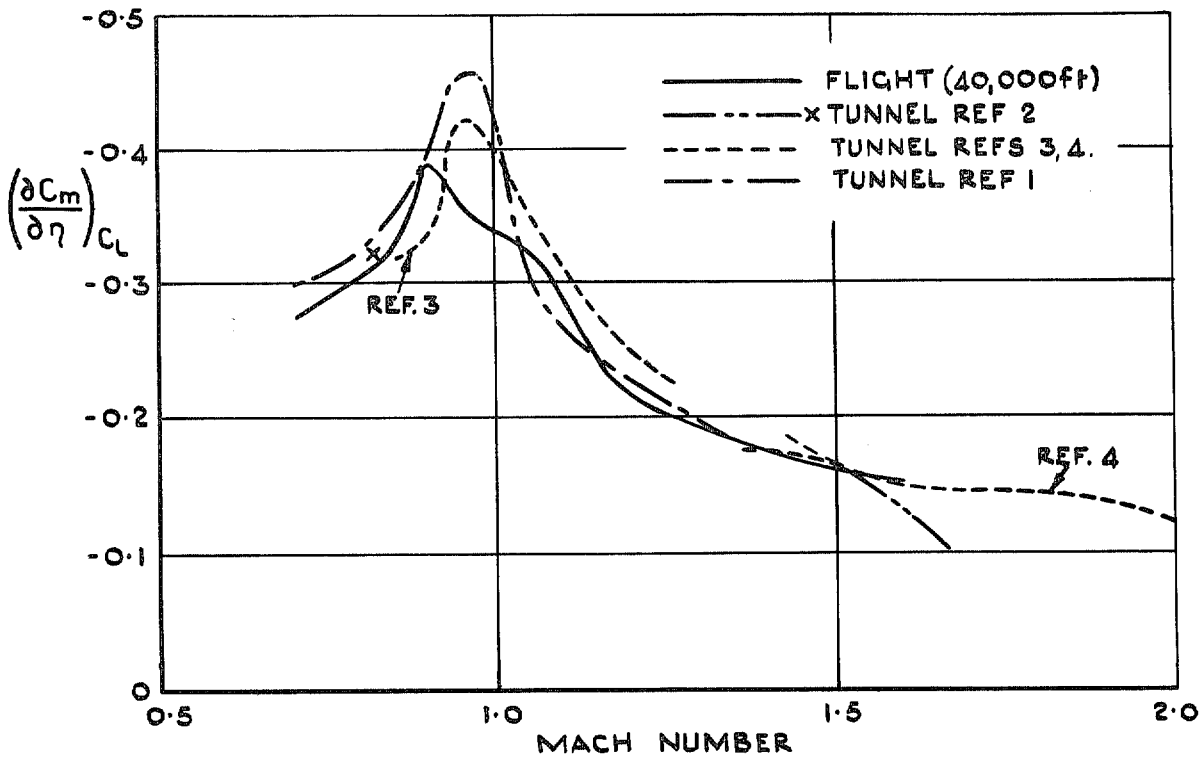

FIG. 15. Variation of elevator pitching power $\left(\frac{\partial C_m}{\partial \eta}\right)_{C_L}$ with Mach number.

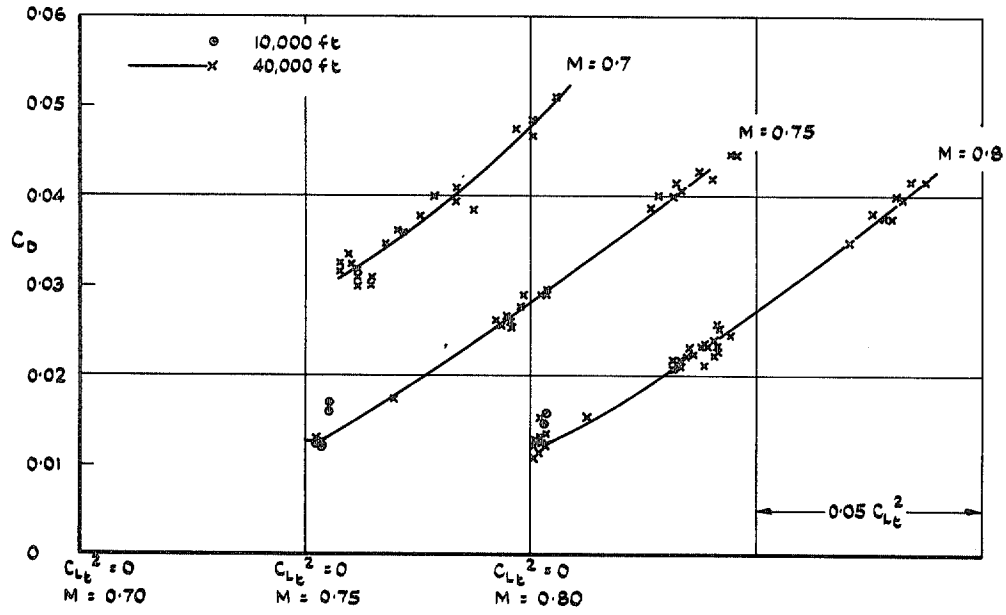

FIG. 18a. Variation of trimmed drag coefficient with $C_{L_t}^2$ for various Mach numbers.

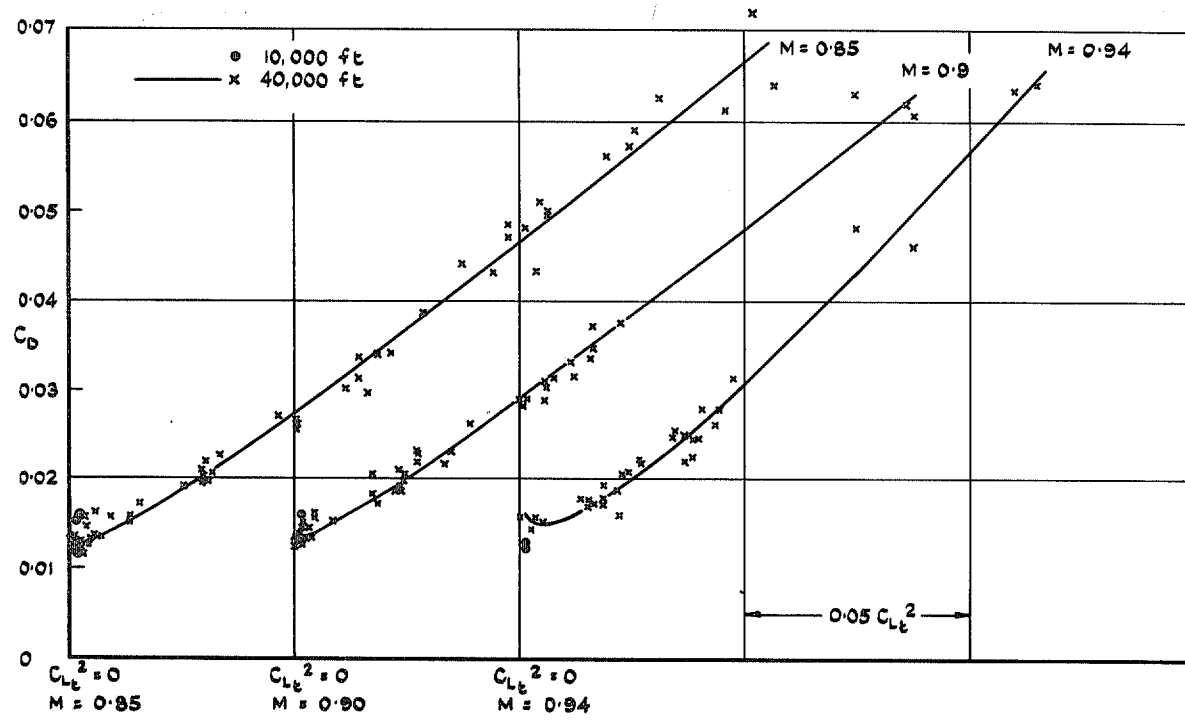

FIG 18b. Variation of trimmed drag coefficient with $C_{L_t}^2$ for various Mach numbers.

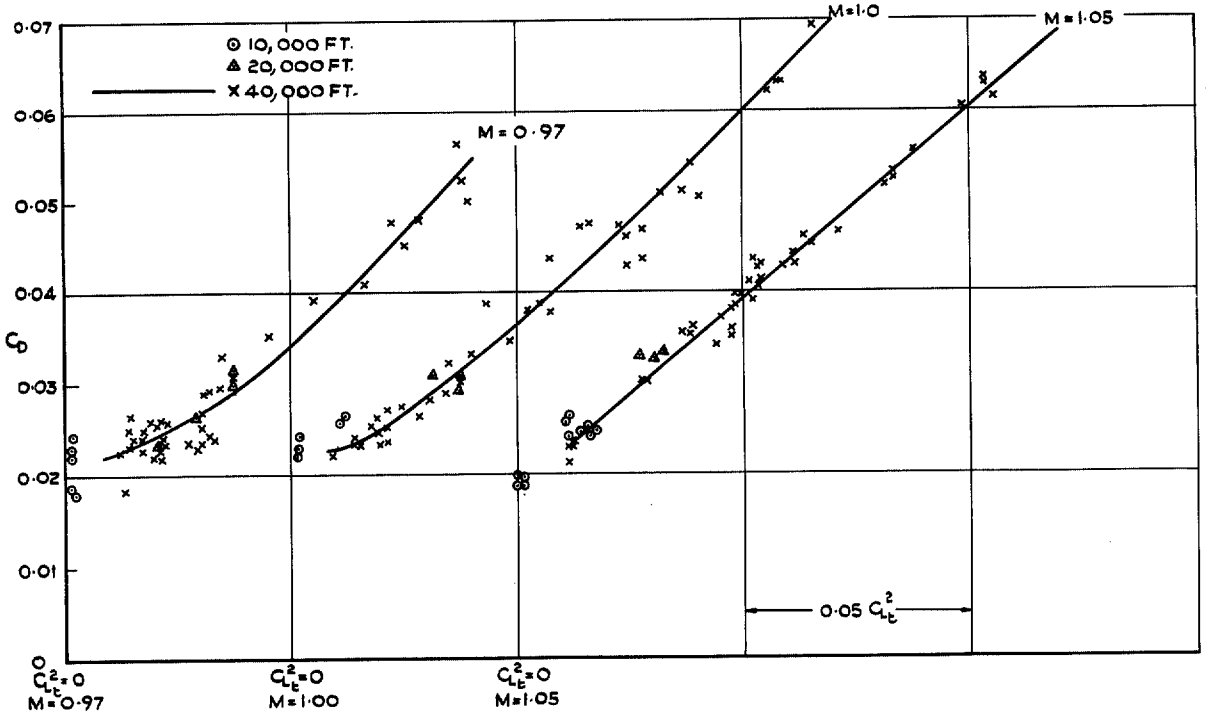

FIG. 18c. Variation of trimmed drag coefficient with $C_{L_t}{}^2$ for various Mach numbers.

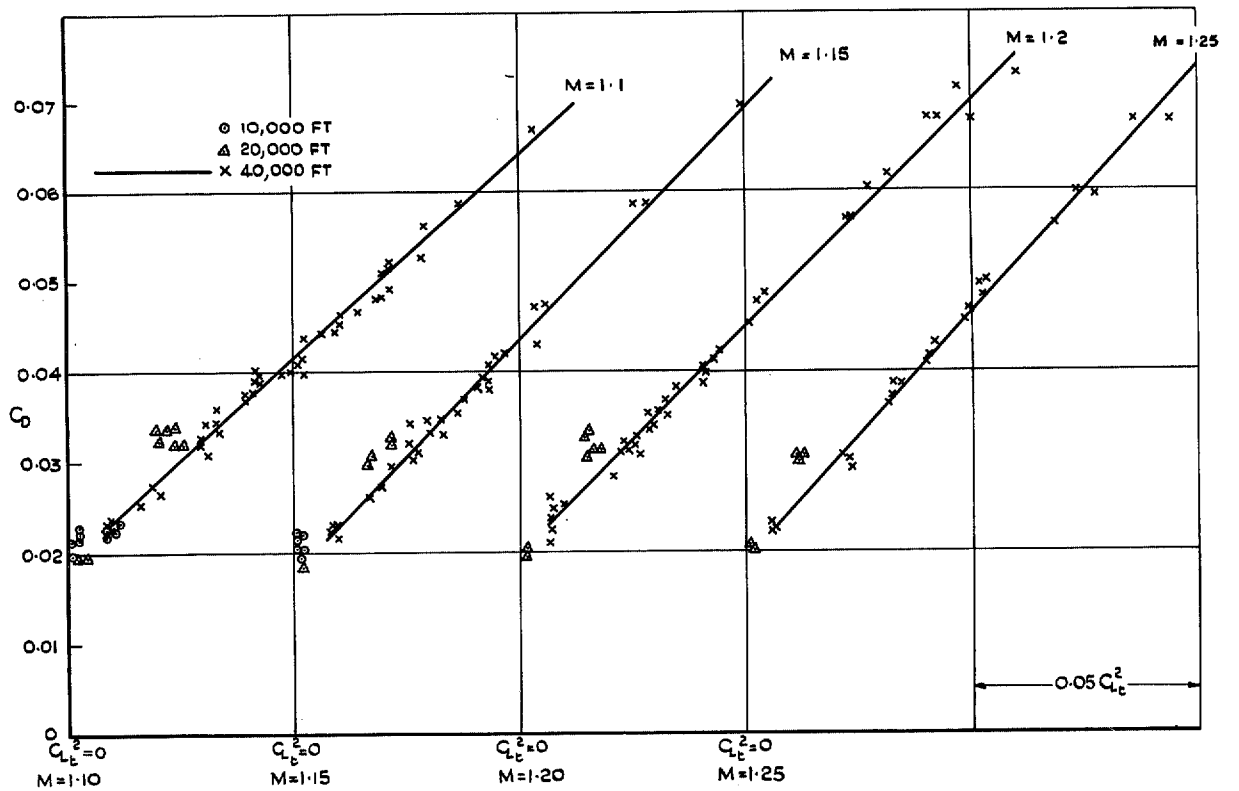

FIG. 18d. Variation of trimmed drag coefficient with $C_{L_t}{}^2$ for various Mach numbers.

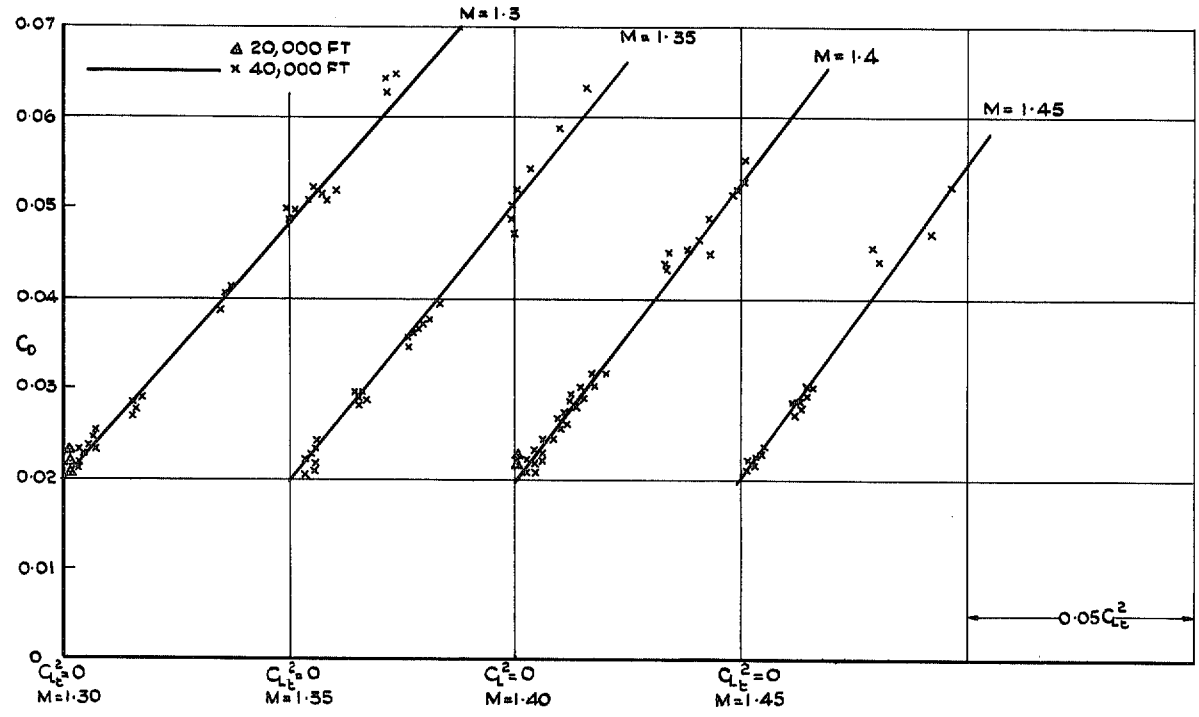

FIG. 18e. Variation of trimmed drag coefficient with $C_{L_t}^2$ for various Mach numbers.

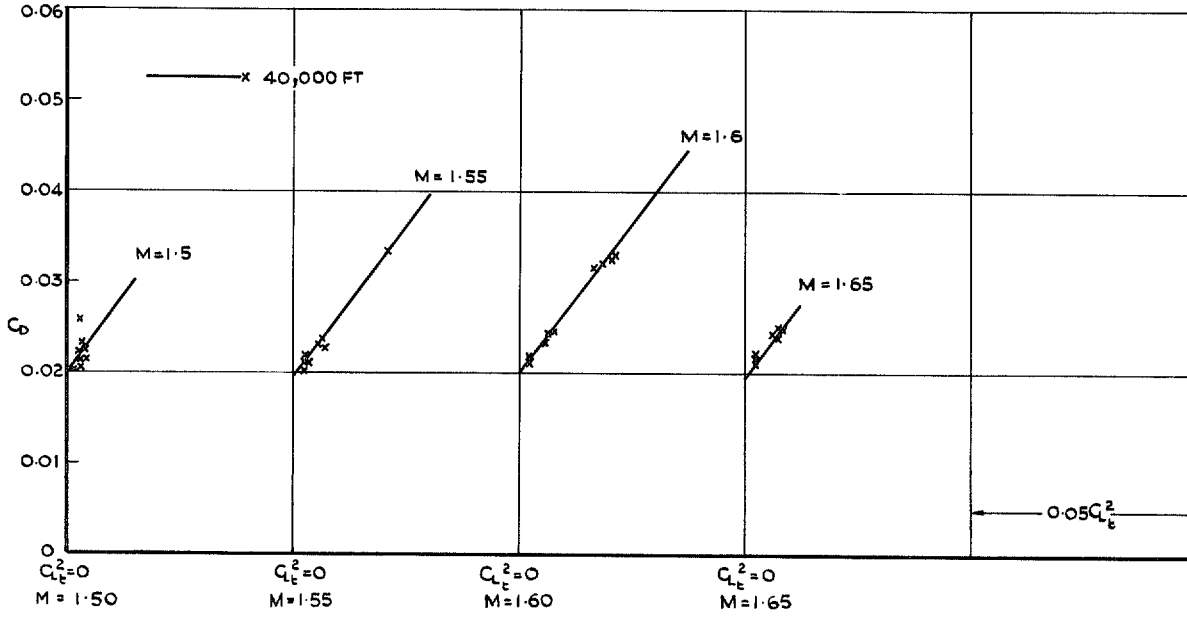

FIG. 18f. Variation of trimmed drag coefficient with $C_{L_t}^2$ for various Mach numbers.

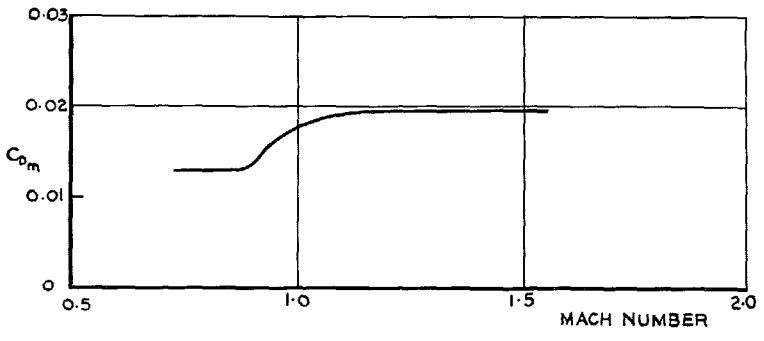

FIG. 19. Variation of minimum drag coefficient C_{D_m} with Mach number.

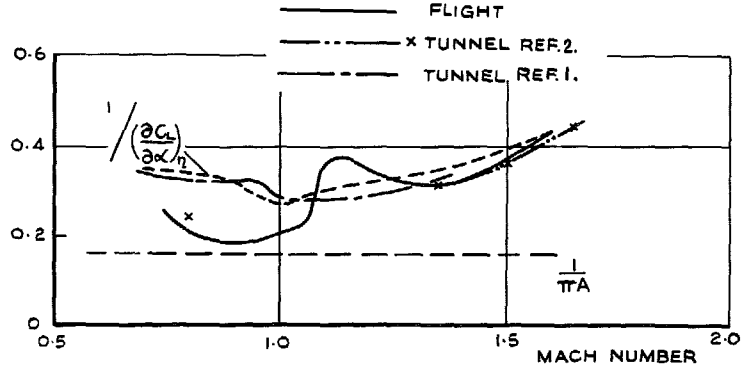

FIG. 20. Variation of the induced-drag factor with Mach number.

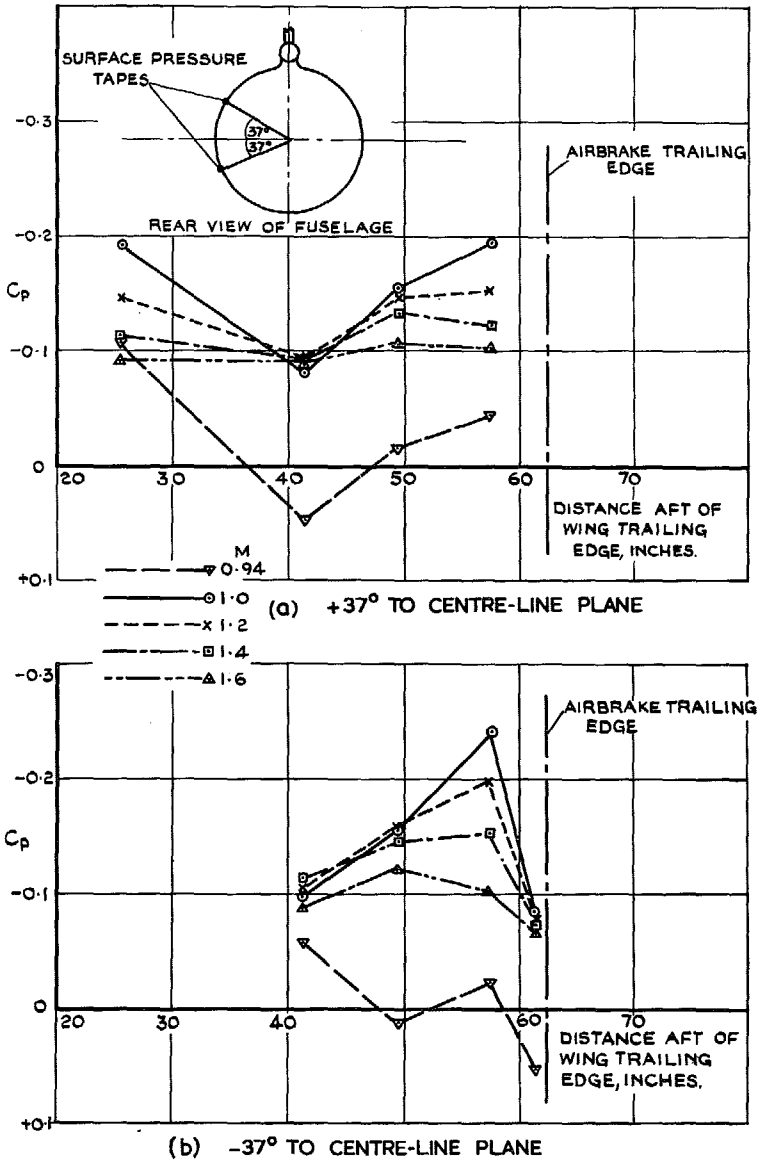

FIG. 21 a & b. Rear fuselage pressures.

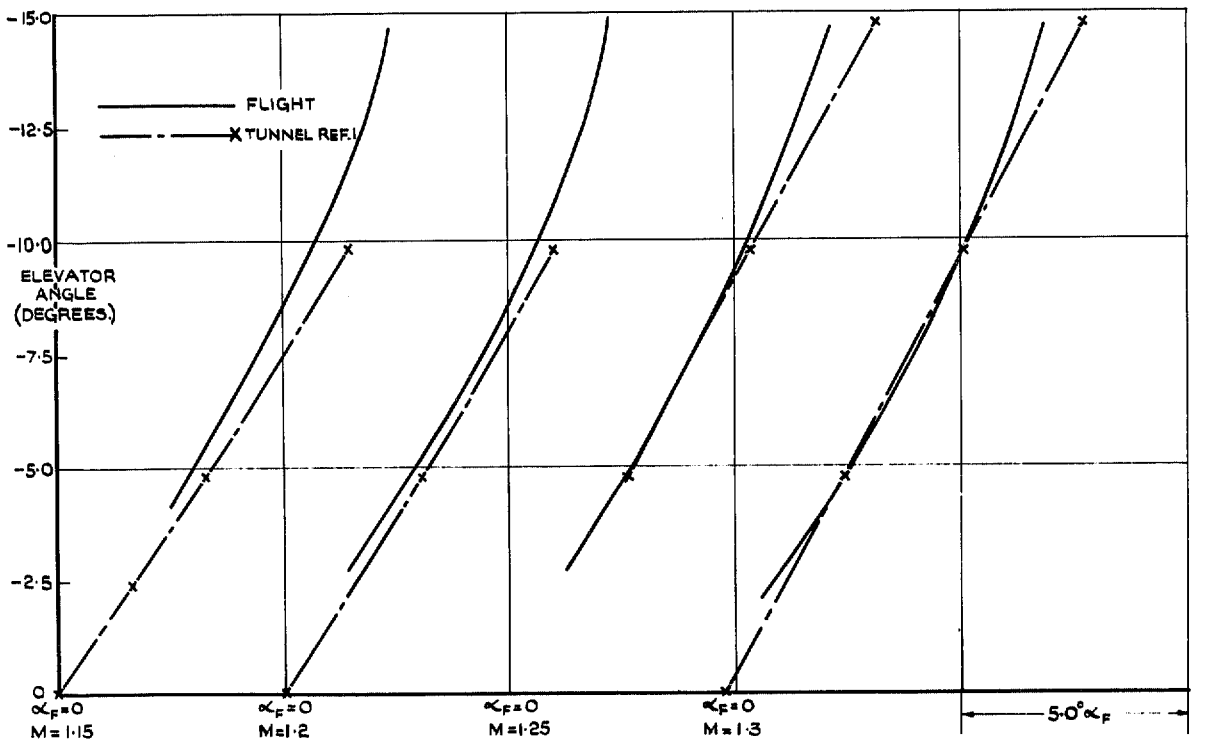

FIG. 22c. Comparison of flight and tunnel elevator angles to trim.

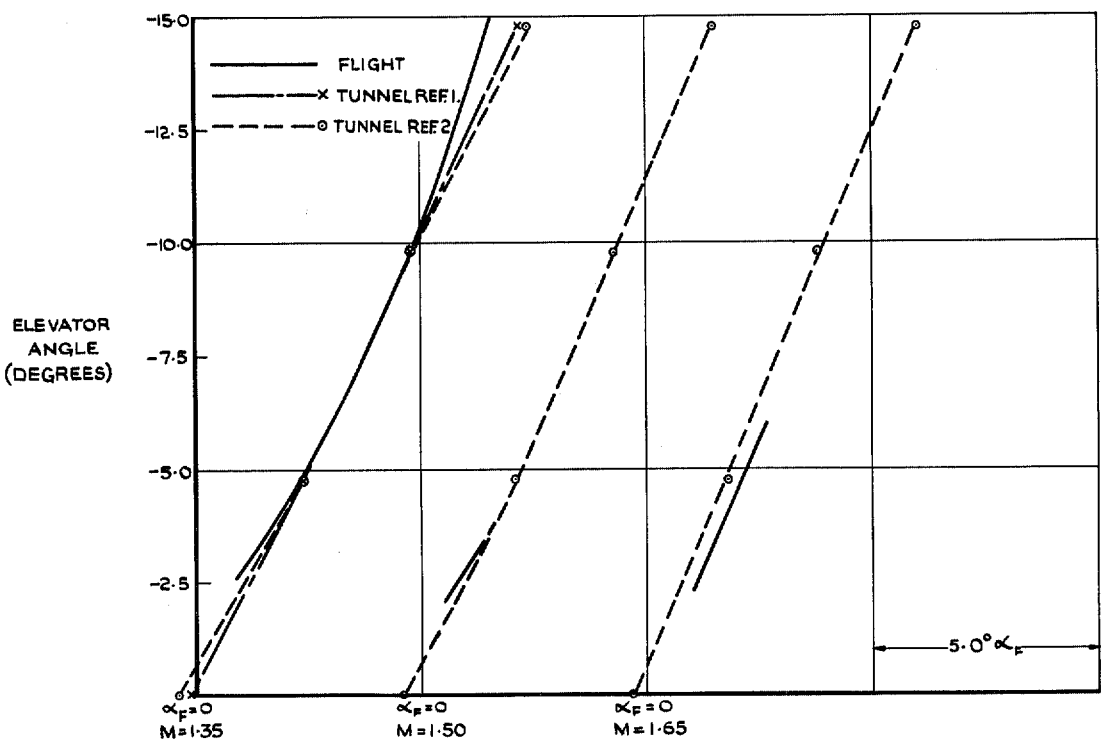

FIG. 22d. Comparison of flight and tunnel elevator angles to trim.

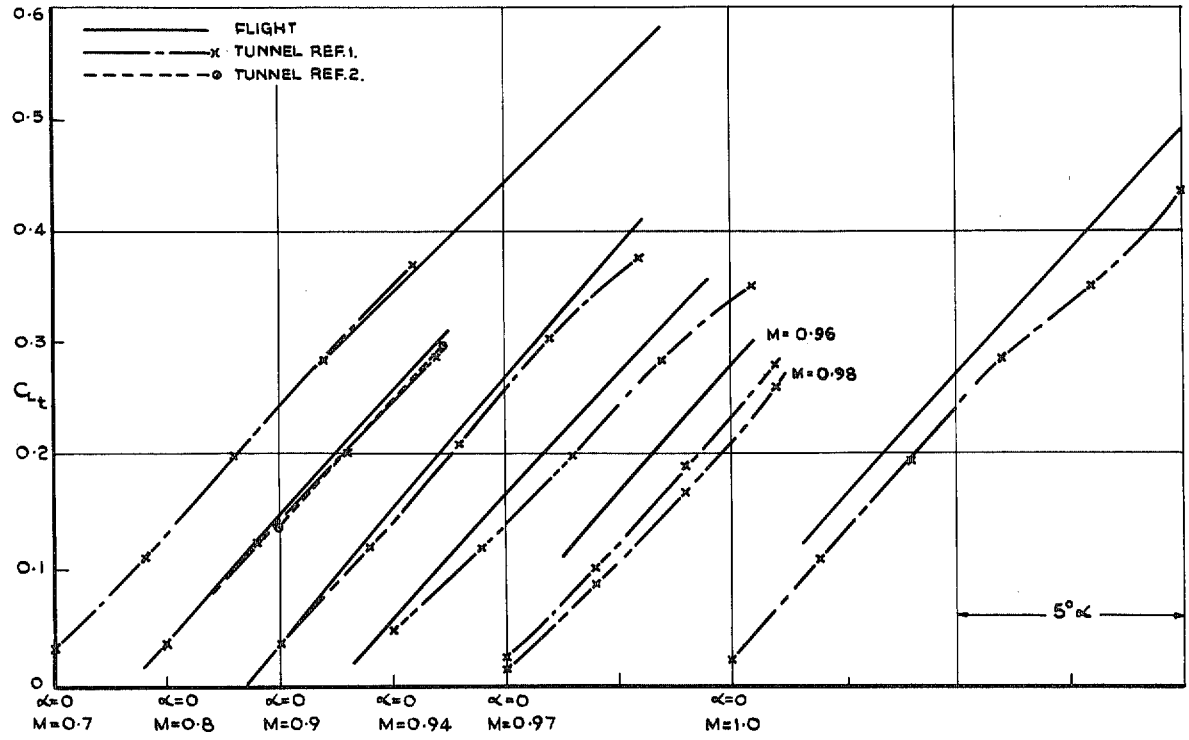

FIG. 23a. Comparison of flight and tunnel trimmed lift data—based on flight values of elevator angles to trim.

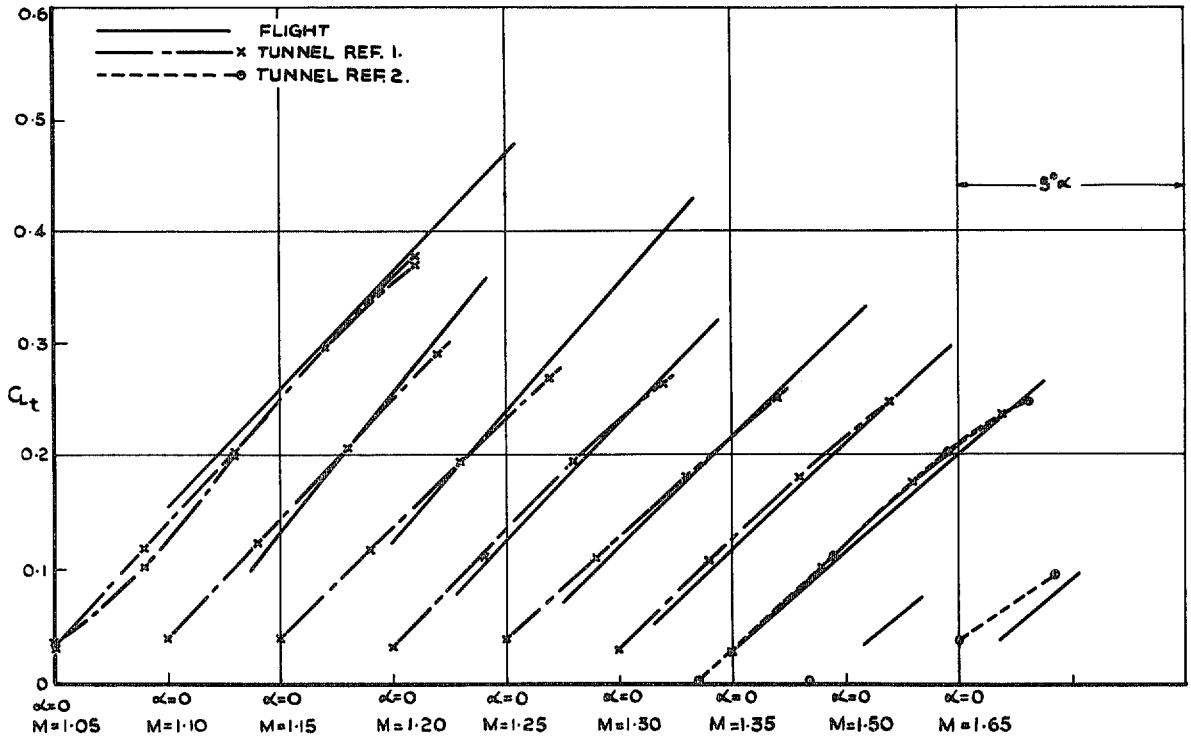

FIG. 23b. Comparison of flight and tunnel trimmed lift data—based on flight values of elevator angles to trim.

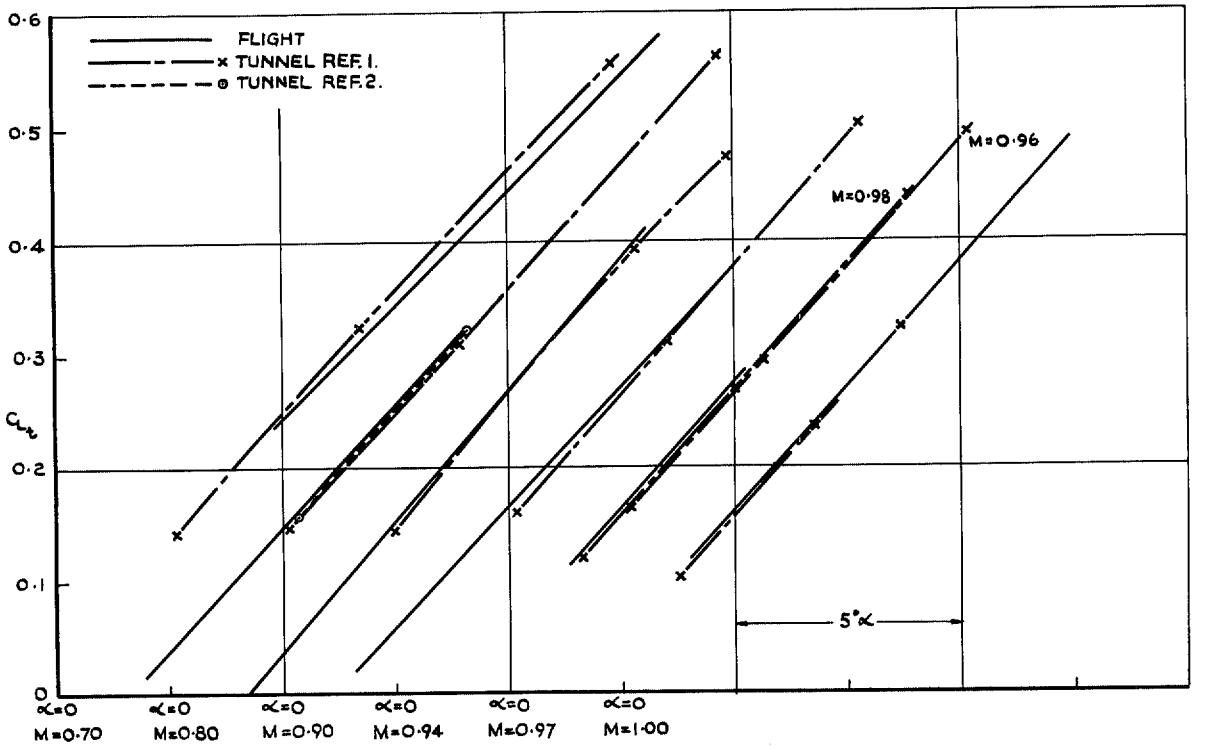

FIG. 24. Comparison of flight and tunnel trimmed lift data as measured.

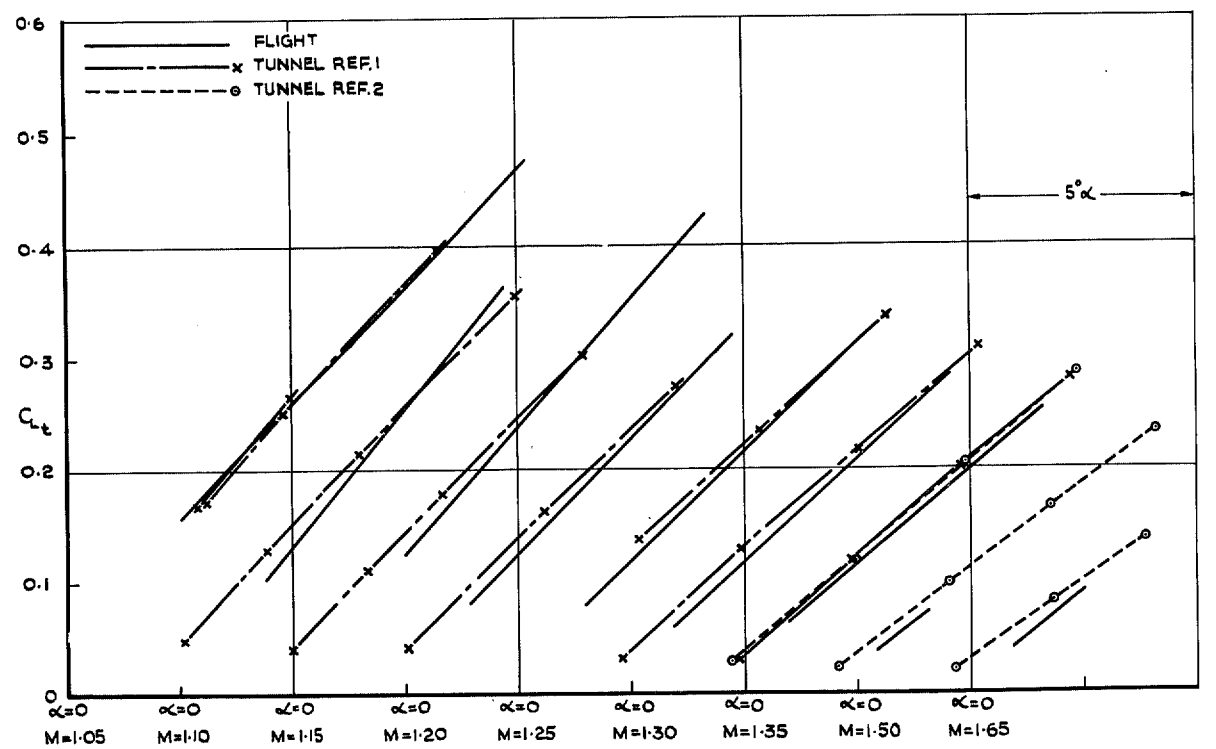

FIG. 24 contd. Comparison of flight and tunnel trimmed lift data as measured.

Printed in Wales for Her Majesty's Stationery Office by Allens Printers (Wales) Ltd.

Dd.135646 K.5.

Published by
HER MAJESTY'S STATIONERY OFFICE

To be purchased from
49 High Holborn, London W.C.1
13A Castle Street, Edinburgh EH2 3AR
109 St. Mary Street, Cardiff CF1 1JW
Brazennose Street, Manchester M60 8AS
50 Fairfax Street, Bristol BS1 3DE
258 Broad Street, Birmingham 1
7 Linenhall Street, Belfast BT2 8AY
or through any bookseller

R. & M. No. 3577
SBN 11 470196 2